OPEN ACCESS

July-September 2019
ISSN 2141-6613
DOI: 10.5897/IJWREE
www.academicjournals.org

ACADEMIC JOURNALS
expand your knowledge

ABOUT IJWREE

The International Journal of Water Resources and Environmental Engineering is published monthly (one volume per year) by Academic Journals.

International Journal of Water Resources and Environmental Engineering (IJWREE) is an open access journal that provides rapid publication (monthly) of articles in all areas of the subject such as water resources management, waste management, ozone depletion, Kinetic Processes in Materials, strength of building materials, global warming etc. The Journal welcomes the submission of manuscripts that meet the general criteria of significance and scientific excellence. Papers will be published shortly after acceptance. All articles published in IJWREE are peer-reviewed.

Contact Us

Editorial Office: ijwree@academicjournals.org

Help Desk: helpdesk@academicjournals.org

Website: http://www.academicjournals.org/journal/IJWREE

Submit manuscript online http://ms.academicjournals.me/

Editors

Editorial Board

International Journal of Water Resources and Environmental Engineering

Table of Contents: Volume 11 Number 7 July-September 2019

ARTICLE

Vol. 11(7), pp. 112-119, July-September 2019
DOI: 10.5897/IJWREE2019.0856
Article Number: F57025B61364
ISSN: 2141-6613

http://www.academicjournals.org/IJWREE

ACADEMIC JOURNALS

International Journal of Water Resources and Environmental Engineering

Full Length Research Paper

Finite difference method to design sustainable infiltration based stormwater management system

Thewodros K. Geberemariam

Department of Civil and Urban Engineering, NYU Tandon School of Engineering, P. O. Box 23195 Brooklyn, New York 11202, USA

Received 11 April, 2019; Accepted 18 June, 2019

Infiltration based stormwater best management practices bring considerable economic, social and ecological benefits. Controlling stormwater quantity and quality are primarily important to prevent urban flooding and minimizing loads of pollutants to the receiving waters. However, there have been growing concerns about how the traditional design approach contributes to the failure of infiltration based BMP's that have caused flooding, ponding, prolonged movement of surface water, and frequent clogging, etc. Many of these problems were due to the fact that the current design approaches of stormwater BMP's only focus on surface hydrology and give little or no attention to the underline subsoil permeability rate and other constraints during the design and sizing process. As a result, many newly constructed infiltration based BMP's are failing to function well. This paper presents and demonstrates a new paradigm shift in designing infiltration-based stormwater BMP's by combining subsurface hydrology and undelaying native soil constraints to establish acceptable criteria for sizing infiltration based BMPs.

Key words: Infiltration based BMP's, flood, infiltration, clogging, soil permeability, underdrain, soil saturation rate, drainage basin, urban drainage

INTRODUCTION

Infiltration is the rate at which surface water percolates into the ground. It is often expressed as cm or inches per hour, but the SI unit is m s^{-1}. The infiltration rate depends on a number of factors including soil type, soil moisture, vegetation, and temperature. Typically, the smaller the grains of soil, the more slowly water percolates into the ground. Also, the wetter the ground, the less room there is for water to infiltrate and consequently, the slower the rate (Bauer, 1974; Guo and Gao, 2016). Many methods have been developed to estimate infiltration rates, and better predict runoff from storm events. The following are some of the methods that are commonly used:

1. **Green-Ampt Method:** - The Green-Ampt equation is a physically based model, which can give a good description of the infiltration process. This method for modeling infiltration assumes that a sharp wetting front exists in the soil column, separating soil with some initial moisture content below from saturated soil above. The input parameters required are the initial moisture deficit of the soil, the soil's hydraulic conductivity, and the suction head at the wetting front (Bedient et al., 2008).

E-mail: tgm@nyu.edu.

2. **Curve Number (SCS) Method:** The Natural Resources Conservation Service (NRCS, formerly Soil Conservation Service (SCS)) Curve Number method is most commonly used method in the United States to determine the volume of runoff called rainfall excess. The curve number (CN) is used to combine infiltration losses with surface storage, to determine what portion of rainfall will runoff. It assumes that the total infiltration capacity of a soil can be found from the soil's tabulated Curve Number. During a rain event, this capacity is depleted as a function of cumulative rainfall and remaining capacity. The input parameters for this method are the curve number, the soil's hydraulic conductivity (used to estimate a minimum separation time for distinct rain events), and a regeneration constant that describes the restoration of infiltration capacity during dry periods (Ward and Trimble, 2004).

3. **Horton Infiltration Method:** Horton's concept of infiltration capacity is based on empirical observations showing that infiltration decreases exponentially from an initial maximum rate to some minimum rate over the course of a long rainfall event. It measured at the ground surface. Each of the parameters in the Horton Infiltration Equation is a function of surface texture and vegetative cover type. The infiltration rate can also vary with slope (McCuen, 2005).

The methods briefly discussed above are widely accepted methods. Each of these methods have their benefits and limitations. For this study, the Horton infiltration method has been used and discussed subsequently.

HORTON'S THEORY OF INFILTRATION

Horton's theory is based on the fact that infiltration is faster in dry ground, so as rain continues and the ground becomes wetter, the infiltration rate decreases. The reason why infiltration is faster when the ground is dry is that there are more spaces for the water to fit so capillary forces that pull the water down into the ground are stronger (Philip, 1969; Verma, 1982).

$$(f - f_c) = (f_0 - f_c)e^{-kt} \quad (1)$$

Horton's Equation is the governing heuristic equation for infiltration, where: f = infiltration rate; f_0 = (initial) infiltration rate for dry ground; f_c = (asymptotic) infiltration rate for saturated ground, and k = infiltration constant

The infiltration equation is written with (f - f_c) on the left hand side (rather than isolating f) because it is the excess infiltration rate above the value for saturated ground that diminishes exponentially with time (Pitt and Voorhees, 2010).

Integrating Horton's equation over time gives the total depth of water that has infiltrated, F,

$$F(t) = \int f dt = f_c t + \frac{(f_0 - f_c)}{k}(e^{-kt} - 1) \quad (1)$$

Where: $F(t)$ = infiltration depth in inch (or mm) at time t.

LIMITS TO HORTON'S THEORY

Horton's equation and integral assume that the rainfall rate, R is greater than the infiltration rate throughout the rain. If at any time the rainfall rate is slower than the infiltration rate, the ground will lose some water to lower levels, and Horton's theory must be modified (Philip, 1969; Stafford et al., 2015).

MODEL INFILTRATING STORMWATER

Infiltration can be modeled by a layer of ground in which water enters through the top at a rate, $f = f_{in}$ and leaves through the bottom (into the water table) at a rate f_{out}. As soon as any water is stored in the ground, storage S will be greater than 0 and,

$$f_{out} = f_c \quad (3)$$

The depth of water stored in the layer, S, is equal to the total depth of infiltration, F minus the depth of water that has leaked out the bottom of the layer. Except in very permeable soil (such as sand or gravel, water leaks out the bottom so slowly; it is safe to assume that during any rainfall,

$$S = F - f_c t \quad (4)$$

The infiltration rate, f_{in} is limited by the rainfall rate and by the total amount of stored water in the layer,

$$f_{in} = \min \begin{bmatrix} R \\ (f_0 - f_c)\dfrac{(S_{max} - S)}{S_{max}} + f_c \end{bmatrix} \quad (5)$$

R = Rainfall Rate and S_{max} = maximum depth of water layer can store

Solving Horton's Equation yields the value for S_{max},

$$S_{max} = \frac{f_0 - f_c}{k} \quad (6)$$

The rate at which water is stored in the layer is equal to the infiltration rate minus the outflow rate through the bottom of the layer, or,

$$\frac{dS}{dt} = f_{in} - f_{out} \quad (7)$$

The difficulty with this equation is that Equation (5) for f_{in} is complicated. If rainfall is ever less than the possible infiltration rate, then it is necessary to solve Equuation (7) numerically, using finite difference techniques (Afrin et al., 2016a, b; Lewellyn et al., 2015; Stafford et al., 2015).

FINITE DIFFERENCE TECHNIQUES

The secret of finite difference techniques is to replace derivatives by finite differences. This transforms a differential equation into an arithmetic equation that can be solved easily. Solving a differential equation using finite differences involves several steps (Al-Hamati et al., 2010; Ferguson, 1990).

1. Replace all derivatives with differences.
2. Solve the equation for the unknown (generally the future value).
2. Choose a value for the time step (Δt) or a distance interval.
3. Substitute current values to find the future value of the variable.
4. Iterate, or, update by repeating step 3 as much as needed.

The derivative is defined as,

$$\frac{dS}{dt} = \lim_{\Delta t \to 0} \frac{S(t + \Delta t) - S(t)}{\Delta t} \quad (8)$$

The finite difference technique assumes that the difference equals the derivative. Then we write the infiltration equation, Equation (8) in finite difference form and rearrange to solve for $S(t+\Delta t)$ because it is the only unknown (Krvavica et al., 2018; Kunze and Nielsen, 1982).

FINITE DIFFERENCE INFILTRATION EQUATION

$$S(t + \Delta t) = S(t) + \Delta t(f_{in} - f_c) \quad (9)$$

Finally, overland flow occurs when the rainfall rate is greater than the infiltration rate. In that case,

$$Overland\ flow = R - f_{in} \quad (10)$$

DETERMINATION OF DESIGN STORAGE VOLUME

In designing infiltration based BMPs, the native soil infiltration on the land surface and the design rainfall event dictate the storage volume for the basin. Moreover, the soil water storage capacity beneath the basin sets up the limit for the maximum water depth in the basin including the invert elevation of the underdrain pipe. In most of urban area, infiltration basined BMPs are often placed next to a small, highly paved small urban catchments such as parking lots and business strip. Therefore, the volume-based approach is suitable to predict the peak runoff from such a small urban watershed, and to finding the maximum volume difference between the inflow and outflow volumes under a series of storm events with different durations (Guo, 1999, 2001, 2002, 2003, 2004; Liu et al., 2015). To determine the peak runoff for a small urban watershed, the rational method states:

$$Q_d = \alpha C I_d A \quad (11)$$

Using the Chicago method, the rainfall intensity in Equation (11) can be calculated (Silveira, 2016) as:

$$I_d = \frac{a}{(T_d + b)^n} \quad (12)$$

Where: α= unit conversion factor, equal to 1 for English units, and 1/360 for SI units; C = runoff coefficient, A= watershed area in acres (hectare), I_d = rainfall intensity in inch/hr (mm/hr), T_d = rainfall duration in minutes, Q_d= peak runoff rate in cfs (cms) and a, b, and n= constants on the Intensity- Duration- Frequency (IDF)

Using the above Equations (10, 11 and 12) we can calculate the maximum volume difference between the inflow and outflow volumes under a series of storm events with different duration (Visocky, 1977). The inflow runoff volume is determined by the net rainfall volume as:

$$V_i = \alpha C I_d A T_d \quad (13)$$

The outflow volume can be estimated by the sump inlet capacity as:

$$V_o = QF(T_d) \quad (14)$$

Therefore, the required design storage volume is the difference between Equations 13 and 14. Aided by Equation 1 to 12, the storage volume, V, is obtained as:

$$V_d = (\alpha C I_d A T_d) - QF(T_d) \quad (15)$$

Where: V_d = Design storage volume, A_b = infiltrating area, and α and β = unit conversion factors.

The maximal value of Equation 15 is achieved by setting its first derivative with respect to T_d equal to zero, and it results in:

$$\frac{dV_d}{dT_d} = \left\{CA \propto \left[\frac{-nT_d}{(T_d+b)^{n+1}} + \frac{1}{(T_d+b)^n}\right] - Qf(T_d)\right\} = 0 \quad when\ T_d = T_m \quad (16)$$

In which Tm = the design rainfall duration described by

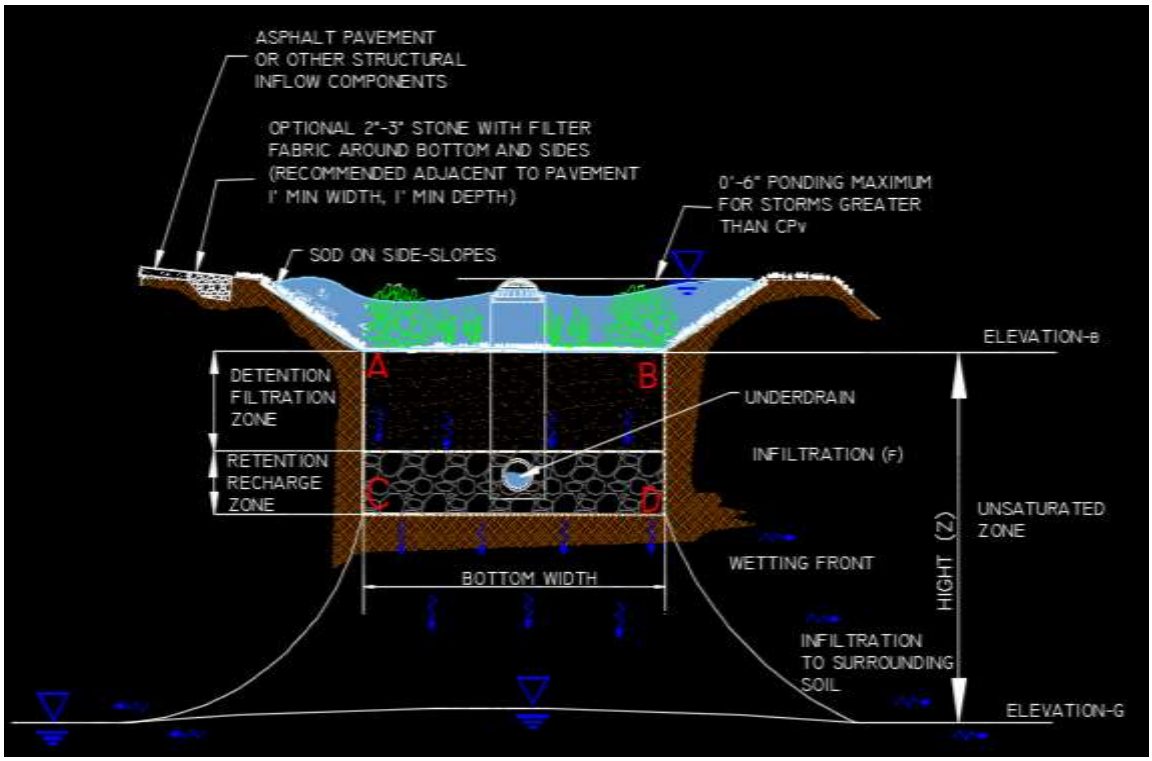

Figure 1. Typical bio-retention infiltration based green infrastructure.

Equation 16. Solution of Equation 16 is:

$$T_m = \frac{1}{n}\left[(T_m + b) - (T_m + b)^{n+1}\frac{Q}{a\alpha CA}\, f(T_m)\right] \quad (17)$$

When the value of b in Equation 16 is numerically negligible, the approximate solution of Equation 16 is:

$$T_m = \left[\frac{2aaCA(1-n)}{Qf(T_m)}\right]^{\frac{1}{n}} \quad (18)$$

Using trial and error of Equation 18 the maximum storage volume, Vm, is

$$V_m = \alpha C I_m A T_m - QF(T_m) \;\; when \;\; T_d = T_m \quad (19)$$

The average infiltration rate, f, through the storm duration is:

$$f = \frac{F(T_m)}{T_m} \quad (20)$$

Where $F(T_m)$ = Total Infiltration depth

SIZING INFILTRATION BASED GREEN INFRASTRUCTURE

The above procedure yields a storage volume based on the surface hydrology without taking the subsurface condition into consideration. If the soil infiltration rate at the land surface is higher than the underground seepage rate, the system is backed up and may even cause a failure in the operation. To be conservative, the water storage volume in soil pores can serve as a limit for the water depth in the basin (Guo, 2004; Miles and Band, 2015; Stafford et al., 2015).

The sample plan view of Infiltration based Green Infrastructure in Figure 1, shows the infiltrating water begins with a vertical downward velocity through the unsaturated zone underneath the basin. As the soil water content increases, the diffusive nature of the wetting front results in flow movements in both vertical and lateral directions (Cannavo et al., 2018; Chu et al., 2018). As soon as the seepage flow reaches the local groundwater table, the soil medium beneath the basin becomes saturated and the seepage flow radially disperses into groundwater. Although many studies used the concept of potential function to investigate the vertical seepage flow and the associated water mounding effect (Guira, 2018)., this study applies stream function to describe the movement of the seepage flow through the soil medium. With the consideration of vertical and radial movements, the potential flow model using stream function is developed for the infiltrating flow under a parabolic infiltration basin (Guo, 1999, 2001) as shown in Figure 1. Infiltration of water into the soil, like many other flow

processes in porous media, is governed by the Richards soil moisture diffusion equation (Celia et al., 1990; Jury et al., 2018; List and Radu 2016). According to the diffusion theory(Green and Ampt, 1911), the seepage flow through the soil medium in Figure 1 can be described as:

$$\frac{\partial\theta}{\partial t}+\frac{\partial f}{\partial z}=0 \quad (21)$$

in which θ = soil moisture content, t = elapsed time, f = infiltration rate, and z = vertical distance below the basin. Consider the soil medium between the basin bottom and groundwater table as a control volume. The finite difference form of Equation 11 is:

$$\Delta\theta=\frac{\Delta f\Delta t}{\Delta z} \quad (22)$$

As illustrated in Figure 1, the value of ∆θ is the difference between the soil initial and saturated moisture contents. The value of ∆z is the depth of the soil medium beneath the basin. The value of ∆f is equal to the infiltration rate from the basin because there is no recharge to the groundwater table before the wetting front reaches the groundwater table. As a result, Equation 21 becomes:

$$(\theta_S-\theta_0)=\frac{(f-0)(T_d-0)}{(Z_b-Z_g)}=\frac{T_d f}{Z} \quad (23)$$

Where, θs = soil porosity, θo = soil initial water content, Zb = elevation at basin bottom, Zg = elevation of groundwater table, Td = drain time, and Z = distance to groundwater table. Re-arranging Equation 23, the drain time at the basin site is derived as:

$$T_d=\frac{Z(\theta_S-\theta_0)}{f} \quad (24)$$

Equation 24 indicates that the drain time of an infiltration basin is dictated by the storage capacity in the soil pores and the infiltration rate. And the water storage volume in the soil pores is equivalent to:

$$d=Z(\theta_s-\theta_0) \quad (25)$$

Where d= equivalent water depth in soil pores. Equation 25 sets the limit for the water depth in the basin. As a result, the footprint surface area of the basin is:

$$A_b=\frac{V_m}{Z(\theta_S-\theta_0)} \quad (26)$$

Equation 19 defines the required storage volume in the basin; Equation 25 sets the maximum water depth in the basin, Equation 26 defines the minimum basin bottom area, and Equation 24 calculates the drain time to release the stored volume. The above design procedure applies to the soil mediums under an unsaturated condition. During an event, the storm water quality control basin may saturate the soil mediums. It is important to understand that the soil medium beneath a retention basin with a permanent pool or a long-term groundwater recharging pond would have saturated already. Under a saturated condition, the major concern in design is no longer the basin geometry, but the basin sub-surface geometry (Healy, 2010; Tedoldi et al., 2016). In other word, we have to make sure that the infiltrating water rate can be sustained by the underground hydraulic gradient and conductivity.

EVALUATION OF THE LONG-TERM SUSTAINABLE PERFORMANCE EFFICIENCY

To evaluate the long-term sustainable of the infiltration based stormwater management system, the designer should analyse the soil medium saturation effect that could reduce the basin infiltration efficiency. As illustrated in Figure 1, the process of infiltration begins with a vertical downward velocity through the unsaturated zone underneath the basin. As the soil water content increases, the diffusive nature of the wetting front results in flow movements in both vertical and lateral directions (Sharma et al., 2018). If the vertical flow through the soil medium is slower than the infiltration rate of the natural soil underneath the infiltration basin, the excess inflow will cause water mounting effect that may back up the system to cause a failure, prolonged draining operation, and minimizing the life-cycle of the basin. Therefore, an infiltrating basin must be designed under the constraints of the soil pore storage capacity before saturation and the soil conveyance capacity after saturation (Haverkamp et al., 1977; Saraswat et al., 2016; Yang and Chui, 2018).

Most of the time the evaluation of the long-term sustainability of the infiltration based stormwater management system based on; analyzing the drain time (I), hydrologic effectiveness (II), required saturated depth (III) and depth of the trench below the underdrain pipe (IV) is as follows.

Analyzing the drain time

Soils must be sufficiently permeable to ensure that collected runoff can infiltrate quickly enough to reduce the potential for flooding and mosquito breeding (that is, water ponding for no more than four days) (Hazelton and Murphy, 2011). Soils with lower hydraulic conductivities do not necessarily preclude the use of infiltration systems, but the size of the required system may typically become prohibitively large, or a more complex design approach may be required, such as including a slow drainage outlet system. Equation 24 indicates that the drain time of an infiltration basin is dictated by the storage capacity in the soil pores and the infiltration rate (Stafford et al., 2015).

Hydrologic effectiveness

The hydrologic effectiveness of an infiltration system defines the proportion of the mean annual runoff volume that infiltrates. For a given catchment area and meteorological conditions, the hydrologic effectiveness of an infiltration system is determined by the combined effect of the nature/quantity of runoff, the 'detention volume', in-situ soil hydraulic conductivity and 'infiltration area (Bracken and Croke, 2007).

The hydrologic effectiveness of an infiltration system requires long term continuous simulation which can be undertaken using the Model for Urban Stormwater Improvement Conceptualization (MUSIC) (CRCCH, 2005). However, in most situations, where a number of the design considerations can be fixed (that is, frequency of runoff, depth of detention storage, and saturated hydraulic conductivity), hydrologic effectiveness curves can be generated and used as the design tool for establishing the infiltration system size (Davis, 2005; Davis et al., 2009).

Depth of the trench below the underdrain pipe

The depth of the trench below the underdrain pipe is dependent on the native soil infiltration rate, porosity (void space ratio) of the gravel storage layer media (that is, aggregate material used in the stone reservoir) and the targeted time period to achieve complete drainage between storm events. The maximum allowable depth below the pipe can be calculated using the following equation (Irvine and Kim, 2018; Kim et al., 2019).

$$D = \frac{i*T*cf}{\eta*s} \quad (27)$$

Where: D = Maximum stone trench depth below pipe (in); I = Infiltration rate for native soils (in/hr.); c_f = clogging factor (0.5); η= Void space ratio for aggregate used (typically 0.4 clear stone); S= Minimum safety correction factor, and T= Time to drain (design for 48-hour time to drain is recommended)

The designer should keep in mind that the determining factor for recharge systems is the surrounding soil's ability to accept water, not the pipe's ability to deliver water. Although the perforations in the pipe determine the allowable area at which water can be released, it is the soil's ability to accept the water that is the determining factor in designing recharge systems.

DESIGN EXAMPLE -1

A 20-lot subdivision in which on-lot structural BMPs provide volume and infiltration for the net increase in volume for the 10-year storm event. Peak rate calculations are developed using techniques described by Equation 12 (Chicago Method) with a = 96.84, b=15.88 and n = 0.7952. The 20-lot subdivision of 5.0 acre is to be developed with a runoff coefficient of 0.75. The 10-year storm runoff from this watershed will drain into 125-ft. by 20-ft. infiltration based green infrastructure basin. The infiltration rates of the basin are: f_o = 2.50 inch/hr., fc = 0.5 inch/hr., and the time constant k = 0.40 /hr. Based on the given information, the design storm duration (min) calculate, the required detention volume (ac-ft.), the total infiltration depth (inch), and the bottom area of the basin (ac) assume α and β are 70 and 1/12, respectively. The following problem can be solved using Equations 2,15 and 17:

1. Calculating the design storm duration (min), using the given data:

$$T_m = \frac{1}{0.7952}\left[(T_m + 15.88) - (T_m + 15.88)^{0.7952+1}\frac{\frac{1}{12} * A_b}{96.84 * 70 * 0.75 * 5} f(T_m)\right]$$

Where: $f(T_m) = 1.2 + (4.5 - 1.2)e^{-\frac{T_m}{60*6.5}}$; Substituting these variables into Equations will yield T_m = 250.00 minute

Calculating the total infiltration depth (inch), and the bottom area of the basin (ac)

$$F(t) = \int f dt = f_c t + \frac{(f_0 - f_c)}{k}(1 - e^{-kt}) \quad \text{and} \quad A_b = \frac{40*100}{43560} \cong 0.092\ ac$$

$$F(t) = 0.5(t) + \frac{(2.5 - 0.5)}{0.4}(1 - e^{-0.4(t)}) \Rightarrow 6.14in$$

Calculating the required detention volume (ac-ft.),

$$V_m = \alpha C I_m A T_m - \beta Q F(T_m) \quad when\ T_d = T_m$$

Substituting these variables into Equations 2, 15, 17 and 19 yields the design storm duration of T_m = 250.00 minute. The total infiltration depth, $F(T_m)$= 6.14 in, the calculated bottom area of the basin = 0.092 ac and the required detention volume for this case is 0.737 acre-ft.

DESIGN EXAMPLE -2

At the project site of Example 1, the soil porosity is 0.50 and has initial water content of 0.20. The distance to the local groundwater table is 8 ft. Designing the basin

geometry for storage volume of 0.737 acre-ft is calculated in example-1. Calculating the maximum stone trench depth below underdrain pipe (in) assume that the void space ratio for clear stone aggregate used is 0.4.

Under the saturated condition, the water storage volume in the 8-ft. soil medium is:

$$d = 8ft.*(0.50-0.20) = 2.40\ feet\ of\ water$$

Assuming that the basin is designed to have the brim-full depth (filled with something to the point of overflowing) of 2.40 feet, the basin area is determined as:

$$A_b = \frac{0.737}{2.40} \cong 0.31\ acre-ft.$$

The final infiltration rate is 0.5 inch/h in Example 1. Therefore, the drain time is:

$$T_d = \frac{2.4*12}{0.5} \cong 36hr.$$

Calculating the maximum stone trench depth below underdrain pipe (in):using Equation 27 the Maximum stone trench depth below underdrain pipe (in) is

$$D = \frac{i*T*cf}{\eta*s} = \frac{0.5*36*0.5}{0.4*05} = 45in \cong use\ 3.75\ ft$$

DESIGN EXAMPLE -3

Given a circular infiltration basin has a diameter of 50.0 ft. The groundwater table at the site is 10.0 feet. The basin will have a layer of loamy sand lining that has an infiltration rate of 1.80 inch/hr. The coefficient of permeability for the native soil is found to be 0.75 inch/hr. Evaluate the sustainability of the proposed infiltration based green infrastructure basin operation, the required saturated distance and suggest that weather the proposed basin lining materials infiltration rate shall be maintained or need revision

Given:

$$Radious\ of\ the\ GI\ basin = r_o = \frac{50}{2} = 25ft.and\ f = 1.80\frac{in}{hr}$$

$$K_r = Ky = K = 0.75\frac{in}{hr}$$

where

$K_r = Hydraulic\ conductivity\ in\ the\ radial\ direction$;
$Ky = Coefficient\ of\ vertical\ permeability, and$
$K = Coefficient\ of\ permeability$

$$Q = f\pi r^2 = \frac{1.80}{12*3600} * 3.1416 * (25)^2 = 0.08\ cfs$$

$$\omega = \frac{1.80}{0.75} = 2.32 \quad where\ \omega = \frac{f}{K_r}$$

$$The\ ratio\ of\ \frac{H}{r_0} = \sqrt{\frac{2.32*ln(2.32)}{2((2.32)^2-1)}} = 0.471 \quad or\ H = 11.78\ ft$$

$$The\ ratio\ of\ \frac{D}{r_0} = 2.32\sqrt{\frac{2.32*ln(2.32)}{2((2.32)^2-1)}} = 1.09 \quad or\ D = 27.25\ ft$$

The required saturated depth calculated as:

$$\frac{Y_0}{r_0} = \frac{D-H}{Y_0} = \xrightarrow{yields} Y_0 = 27.25 - 11.78 = 15.33\ ft.$$

The required saturated distance is greater than the available (15.33 >10.00 ft.). Therefore, the design infiltration rate or the design radius of the GI must be reduced.

Conclusion

On this paper, we assessed what contributes to the failure of most recently constructed infiltration based BMP's such as porous pavements, riprap trenches, infiltration beds, retention pools, detention systems, wetlands, and drywells. Examination of the current design approaches further revealed that the serious negligence of site constraints that have caused flooding, ponding, prolonged movement of surface water, and frequent clogging, etc. This paper demonstrates the need in paradigm shift when designing sustainable infiltration based stormwater management system. Using finite difference method to design infiltration based stormwater management approaches integrates all constraints such as underlying soil permeability (k), drain time (Td), hydrologic effectiveness, and the depth of the trench below the underdrain pipe.

Finally, the evaluation of the sustainability of the proposed infiltration based stormwater management operation shall be dependent on the native soil infiltration rate, porosity (void space ratio) of the gravel storage layer media (trhat is, aggregate material used in the stone reservoir) and the targeted time period to achieve complete drainage between storm events. No single method works well for all situations.

CONFLICT OF INTERESTS

The authors have not declared any conflict of interests.

REFERENCES

Afrin T, Kaye NB, Khan AA, Testik FY (2016). Parametric study of perforated pipe underdrains surrounded by loose aggregate. Journal of Hydraulic Engineering 142(12):04016066.

Afrin T, Khan AA, Kaye NB, Testik FY (2016). Numerical model for the hydraulic performance of perforated pipe underdrains surrounded by loose aggregate. Journal of Hydraulic Engineering 142(8):04016018.

Al-Hamati AA, Ghazali AH, Mohammed TA (2010). Determination of storage volume required in a sub-surface stormwater detention/retention system. Journal of Hydro-environment Research 4(1):47-53.

Bauer SW (1974). A modified Horton equation for infiltration during intermittent rainfall. Hydrological Sciences Journal 19(2):219-225.

Bedient PB, Huber WC, Vieux BE (2008). Hydrology and floodplain analysis.

Bracken LJ, Croke J (2007). The concept of hydrological connectivity and its contribution to understanding runoff-dominated geomorphic systems. Hydrological Processes 21(13):1749-1763.

Cannavo P, Coulon A, Charpentier S, Béchet B, Vidal-Beaudet L (2018). Water balance prediction in stormwater infiltration basins using 2-D modeling: An application to evaluate the clogging process. International Journal of Sediment Research 33(4):371-384

Celia MA, Bouloutas ET, Zarba, RL (1990). A general mass-conservative numerical solution for the unsaturated flow equation. Water resources Research 26(7):1483-1496.

Chu X, Jia X, Liu Y (2018). Quantification of wetting front movement under the influence of surface topography. Soil Research 56(4):382-395.

Davis AP. (2005). Green engineering principles promote low-impact development.

Davis AP, Hunt WF, Traver RG, Clar M (2009). Bioretention technology: Overview of current practice and future needs. Journal of Environmental Engineering 135(3):109-117.

Ferguson BK (1990). Role of the long-term water balance in management of stormwater infiltration. Journal of Environmental Management 30(3):221-233.

Green WH, Ampt GA (1911). Studies on Soil Phyics. The Journal of Agricultural Science 4(1):1-24.

Guira M (2018). Numerical modeling of the effects of land use change and irrigation on stream flow depletion of Frenchman creek, Nebraska.

Guo JC (1999). Detention storage volume for small urban catchments. Journal of Water Resources Planning and Management 125(6): 380-382.

Guo JC, Urbonas B (1999). Maximized detention volume determined by runoff capture ratio. Journal of Water Resources Planning and Management 122(1):33-39**.**

Guo JC (2001). Design of circular infiltration basin under mounding effects. Journal of Water Resources Planning and Management 127(1): 58-65.

Guo, JC (2002). Overflow risk of storm water BMP basin design. Journal of Hydrologic Engineering 7(6):428-434.

Guo JC (2003). Design of infiltrating basin by soil storage and conveyance capacities. Water International 28(4):411-415

Guo JC (2004). Hydrology-based approach to storm water detention basin design using new routing schemes. Journal of Hydrologic Engineering 9(4):333-336.

Guo JC, Hughes W (2001). Runoff Storage Volume for Infiltration Basin. Journal of Irrigation and Drainage Engineering 127(3):170-174.

Guo JC, Urbonas B (2002). Runoff capture and delivery curves for storm-water quality control designs. Journal of Water Resources Planning and Management 128(3): 208-215.

Guo Y, Gao T (2016). Analytical equations for estimating the total runoff reduction efficiency of infiltration trenches. Journal of Sustainable Water in the Built Environment *2*(3):06016001.

Haverkamp R, Vauclin M, Touma J, Wierenga PJ, Vachaud G (1977). A Comparison of Numerical Simulation Models for One-Dimensional Infiltration 1. Soil Science Society of America Journal 41(2):285-294.

Hazelton P, Murphy B (2011). Understanding soils in urban environments. Csiro Publishing.

Healy RW (2010). Estimating groundwater recharge. Cambridge University Press.

Irvine JL, Kim AS. (2018). Understanding bioswale as a small water and wastewater treatment plant: A theoretical review. Desalination and Water Treatment 1:15.

Kim H, Mallari KJB., Baek J, Pak G, Choi HI, Yoon J (2019). Considering the effect of groundwater on bioretention using the Storm Water Management Model. Journal of Environmental Management 231:1270-1276.

Krvavica N, Jaredić K, Rubinić J (2018). Methodology for defining the design storm for sizing the infiltration system. Građevinar 70(08):657-669.

Kunze RJ, Nielsen DR (1982). Finite-difference solutions of the infiltration equation. Soil Science 134(2):81-88.

Lewellyn C, Lyons CE, Traver RG, Wadzuk BM (2015). Evaluation of seasonal and large storm runoff volume capture of an infiltration green infrastructure system. Journal of Hydrologic Engineering 21(1):04015047.

List F, Radu FA (2016). A study on iterative methods for solving Richards' equation. Computational Geosciences 20(2):341-353.

Liu W, Chen W, Peng C (2015). Influences of setting sizes and combination of green infrastructures on community's stormwater runoff reduction. Ecological Modelling 318:236-244.

McCuen RH (2005). Accuracy assessment of peak discharge models. Journal of Hydrologic Engineering, *10*(1): 16-22.

Miles B, Band LE (2015). Green infrastructure stormwater management at the watershed scale: urban variable source area and watershed capacitance. Hydrological Processes 29(9):2268-2274.

Philip J R (1969). Theory of infiltration. In: Advances in hydroscience Elsevier 5:215-296.

Pitt R, Voorhees J (2010). Integrated modeling of green infrastructure components in an area served by combined sewers. In Low Impact Development 2010: Redefining Water in the City, pp: 1617-1630.

Saraswat C, Kumar P, Mishra BK (2016). Assessment of stormwater runoff management practices and governance under climate change and urbanization: An analysis of Bangkok, Hanoi and Tokyo. Environmental Science and Policy 64:101-117.

Sharma A, Gardner T, Begbie D (Eds.) (2018). Approaches to Water Sensitive Urban Design: Potential, Design, Ecological Health, Urban Greening, Economics, Policies, and Community Perceptions. Woodhead Publishing.

Silveira ALLD (2016). Cumulative equations for continuous time Chicago hyetograph method. RBRH 21(3):646-651.

Stafford N, Che D, Mays LW (2015). Optimization model for the design of infiltration basins. Water Resources Management 29(8):2789-2804.

Tedoldi D, Chebbo G, Pierlot, D, Kovacs Y, Gromaire MC (2016). Impact of runoff infiltration on contaminant accumulation and transport in the soil/filter media of Sustainable Urban Drainage Systems: A literature review. Science of the Total Environment 569:904-926.

Verma SC (1982). Modified Horton's infiltration equation. Journal of Hydrology 58(3-4):383-388.

Visocky AP (1977). Hydrologic Study of Illinois Beach State Park. Circular no. 128

Ward AD, Trimble SW, Burckhard SR, Lyon JG. (2004). Environmental hydrology (Vol. 464). Florida^ eBoca Raton Boca Raton: Lewis Publishers.

Yang Y, Chui TFM (2018). Rapid assessment of hydrologic performance of low impact development practices under design storms. JAWRA Journal of the American Water Resources Association 54(3):613-630.

Vol. 11(7), pp. 120-128, July-September 2019
DOI: 10.5897/IJWREE2019.0857
Article Number: C99932861552
ISSN: 2141-6613

http://www.academicjournals.org/IJWREE

ACADEMIC JOURNALS
expand your knowledge

International Journal of Water Resources and Environmental Engineering

Full Length Research Paper

Evaluation of the current water quality of Lake Hawassa, Ethiopia

Haile Melaku Zigde* and Mohammed Endale Tsegaye

Department of Chemistry, College of Natural and Computational Science, Hawassa University, Hawassa, Ethiopia.

Received 1 May, 2019; Accepted 17 June, 2019

The research aimed to evaluate the current wáter quality of Lake Hawassa in order to identify potential pollution sources and suggest appropriate measures. Physico-chemical water quality parameters have been determined by taking duplicate samples from seven sampling sites and the results were compared with WHO and FAO standards. The findings of the study revealed that the concentration of metals such as manganese (0.83 mg/L), zinc (5.75 mg/L), chromium (0.22 mg/L), phosphate (1.31 mg/L), and biochemical oxygen demand 5 (BOD5, 68.7 mg/L) exceeded WHO standard that could be due to point sources pollution from ceramics, textile, plastics, leather tanning and food processing industries located near the rivers and streams that end up into the lake. Moreover, the study indicated that the lake has also been polluted by non-point source pollution caused by urban stormwater, agricultural runoff, over grazing, deforestation, soil erosion and land development as it was shown with elevated levels of total dissolved solids (TDS, 928.3 mg/L), electrical conductivity (EC, 1851.4 µS/cm), turbidity (47.9 NTUs), fluoride (15.3 mg/L) and potassium (74.2 mg/L). Therefore, intervention measures should be put in place to prevent pollution of the lake.

Key words: Ethiopian Rift Valley Lakes, surface water pollution, water quality parameters, nutrients, metals.

INTRODUCTION

The Ethiopian Rift Valley Lakes (ERVLs) are water resources characterized by a chain of lakes varying in size, hydrological and hydrogeological settings. It constitutes seven main fresh and saline lakes, such as Lake Ziway, Lake Langano, Lake Abiyata, Lake Shalla, Lake Hawassa, Lake Abaya, and Lake Chamo. Among these lakes, Lake Hawassa is the smallest fresh water closed basin lake and is used for various purposes such as small-scale commercial fishing, recreation, irrigation, etc., by semi-urban and urban dwellers (Gebremedhin and Berhanu, 2015; Zinabu and Zerihun, 2002). However, the lake encounters a high risk of pollution from anthropogenic activities, such as urbanization, intense agriculture, rapid industrialization, urban runoff and natural activities such as erosion and heavy rainfall (Katie, 2011; Larissa et al., 2012). Particularly, those industries housed in Hawassa Industrial Park (HIP) and others have been known to release effluents into rivers and streams that end up into the swampy area of the former Lake Shallo from which River Tikurwhua originates (Zinabu and Zerihun, 2002) and fed the lake. This is an immediate threat to the community that uses

*Corresponding author. E-mail: melerevised@gmail.com. Tel: (+251)912371675.

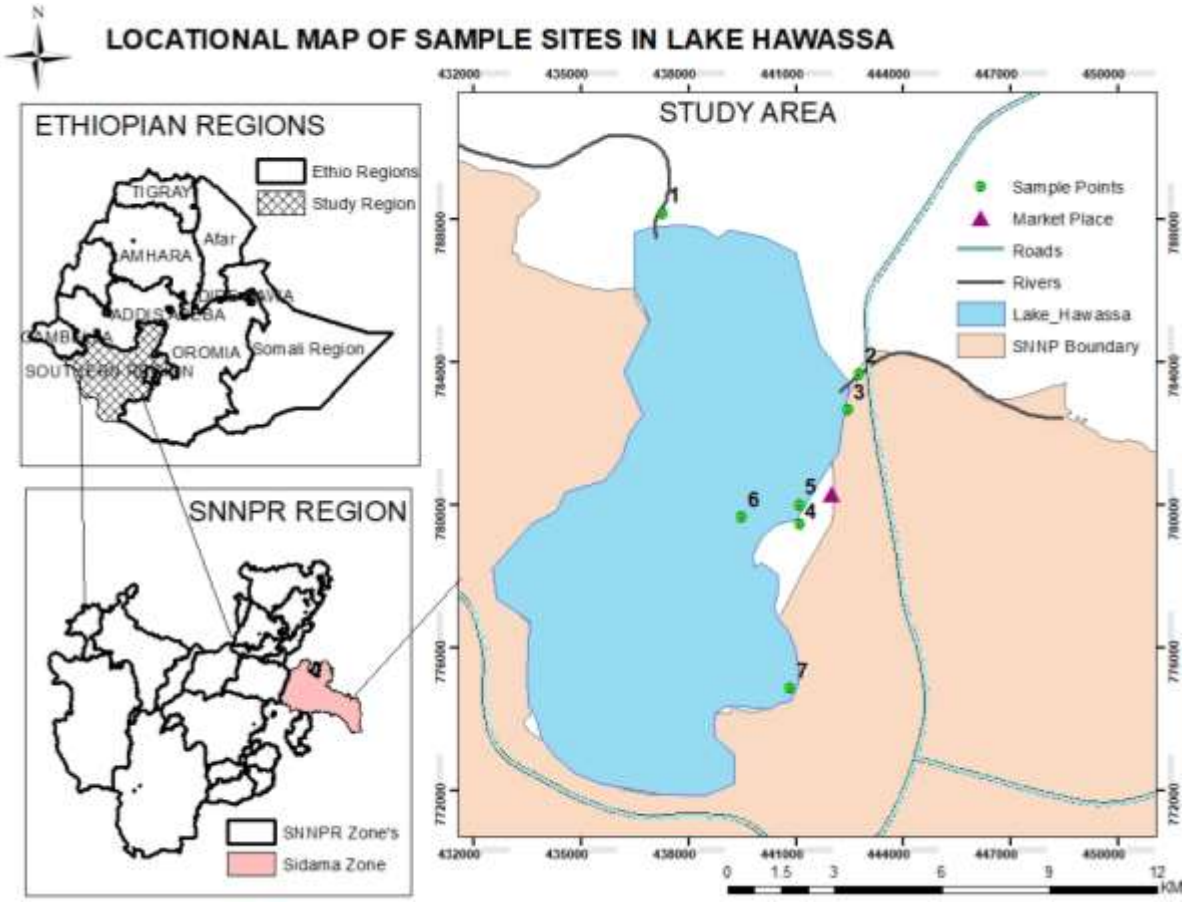

Figure 1. Location map of sample sites in Lake Hawassa.

the rivers and streams for various purposes and to the survival of aquatic life and for the long term survival of the lake. Furthermore, the lake faces a high risk of pollution as a result of natural activities, such as erosion and heavy rainfall. Therefore, the research focussed on assessing the current water quality of Lake Hawassa in order to identify potential pollution sources and suggest appropriate measures by analysing physico-chemical water quality parameters such as pH, temperature, total dissolved solids (TDS), dissolved oxygen (DO), turbidity, electrical conductivity (EC), biochemical oxygen demand (BOD), total hardness, total alkalinity, nutrients and concentration of major and minor metal ions for selected sampling sites.

MATERIALS AND METHODS

Description of the study area

This study was carried out in Lake Hawassa, the smallest and the highest in altitude among the Rift valley closed basin lakes, located between 06°58′ to 07° 14′ North latitudes and 38° 22′ to 38° 28′ East longitudes with an elevation of 1697 m above sea level and its annual rainfall average is 969 mm (HALCROW, 2008). The lake is a shallow lake with average depth of 13.3 m and maximum depth of 23.4 m (Mulugeta, 2013). It has a surface area of 90 km^2 and a drainage area of 1250 km^2 (Girma and Ahlgren, 2009) and a water storage capacity of the lake is 1.36 km^3 (Ayenew et al., 2007). The lake is fed by TikurWuha River, a perennial river that drains water from eastern escarpment and a swampy area of the former Lake Shallo (Chaleleka) (Makin et al., 1975). According to Legesse et al. (2003), the climate in Lake Hawassa region is characterized by three main seasons: long rainy season in the summer from June to September is known locally as Kiremt, dry season (locally named as baga) extends between October and February, and "small rain" season (locally named as belg) extends between March and May. The mean annual rainfall is variable ranging from 600 to 1200 mm with a mean value of 961 mm and distributed as 50% for Kiremt (June-September); 20% for baga (October-February) and 30% for belg season (March-May). Due to limited time, money and preliminary observation, a total of seven sampling sites, namely SLW1, SLW2, SLW3, SLW4, SLW5, SLW6, and SLW7 were selected as shown in Figure 1. Five of the total sampling sites were selected within the boundaries of the lake and an additional two sampling sites were selected at the entry point of rivers. The selected sampling sites code, name, and geographical locations are shown in Table 1.

Sampling, sample preparation and analysis

Samples were collected in duplicate and a total of fourteen water

Table 1. Sampling sites code, name, and geographical locations.

Sampling site	Name of sampling site	(GPS)		
		Altitude, m	Latitude (degree, min, s)	Longitude (degree, min, s)
SLW1	Near new Air port	1694	07°07'48.0''	038 °25'55.1''
SLW2	Tikur Wuha River	1672	07°08.4'8.8''	038 °28.9'3.1''
SLW3	Near Haile Resort	1684	07°04.7'7.1''	038 °28.6'8.3''
SLW4	Fikir Hayik	1687	07°03'4.91''	038 °28'.060''
SLW5	Fikir Hayik Marsh	1684	07°03'.21.9''	038 °28'.006''
SLW6	Near Lewi Resort	1683	07°03'011''	038 °27'.7.93''
SLW7	Around Loke	1684	07°00'34.6''	038 °27'52.1''

samples were collected from the selected sampling sites during the belg season (March and April) in 2019. The samples were collected in 1 L capacity plastic bottles and preserved airtight to avoid evaporation. Physical parameters such as TDS, SC, and temperature were determined *in situ* using a Wagtech Conductivity-/-TDS Meter. DO was determined in situ using a HANA Model HI 9143 dissolved oxygen meter. Turbidity and pH were determined onsite using a Wagtech turbidimeter, and a pH meter, respectively. BOD was determined at 20°C for 5 days period using standard method (Delzer and McKenzie, 2003).

These samples were kept refrigerated at -4°C prior to the analysis of nutrients, major and trace metals. Major ions such as K^+ and Mg^{2+} and trace metals such as iron were determined using Photometer 7100 integrated with the Palintest system of water analysis, which uses a reagent systems in tablet or liquid tubetests that react with metal ions to produce either a color or turbid solution so that direct readings in concentration units is possible (Photometer 7100 instruction manual). Fluoride and nutrients such as nitrate, sulfate, and phosphate were determined using Photometer 7100 integrated with the Palintest system of water analysis. Total alkalinity was determined by acid titration with 0.02 N H_2SO_4 and total hardness was determined by ethylenediamine tetra acetic acid (EDTA) titration.

Trace metals such as Mn, Cu, Zn, Cr, and Pb were determined using atomic absorption spectrophotometer (Buck Scientific, Model 210 VGP Atomic absorption spectrophotometer, USA). For the analyses of trace metals, 100.0 mL of unfiltered water sample was taken in a beaker and heated until the volume of the sample solution reached 20.0 mL. Then, the sample solution was cooled and acidified with 2.0 mL of concentrated nitric acid and filtered into a 100.0 mL volumetric flask and made up to the mark with deionized water. Then, the analyses were completed using an atomic absorption spectrophotometer.

Statistical analysis

Descriptive statistics for the selected physico-chemical water quality parameters were carried out. And a one-way analysis of variance (ANOVA) with a post hoc multiple comparisons (Tukey's test) were used to compare the mean values of results obtained for each sampling sites. The results were compared with WHO and FAO standards.

RESULTS AND DISCUSSION

Physical water quality parameters

The physical water quality parameters investigated is listed in Table 2. High variations in mean values of physical parameters among sites were observed for EC, TDS, and Turbidity. The mean values of the selected physical parameters ranged between 741.7 and 1956.0 µS/cm for EC, 383.7 and 979.3 mg/L for TDS, 8.37 and 177.0 NTUs for turbidity, 5.85 and 9.21 for pH, 4.76 and 8.59 mg/L for dissolved oxygen, 20.6 and 28.3°C for temperature.

pH

Statistical analysis showed that the mean values of pH were significantly different at 95% confidence level among sampling sites. Higher values above the limits were observed at SLW1, SLW3, SLW4, and SLW7 sampling sites. The high value of pH at these sampling sites was attributed to the geological formation of soil reach in carbonates added to the water through erosion and causing the lake to be alkaline. The high pH and the corresponding alkalinity in this study was in agreement with previous study (Ayenew, 2007) findings in which crater lakes are often alkaline where alkalinity is a measure of fertility of the lake at this range rather than pollution indicator. The pH value at SLW5 sampling site (stagnant water near the lake) was slightly acidic (5.85) and below the (WHO, 2004) limits. This might be due to the dissolution of carbon dioxide and nutrients produced during bacterial decomposition of food waste and sewage waste near the lake (Walakira and Okot-okumu, 2011).

Temperature

Temperature is one of the most important physical factors affecting the chemical and biological reaction in water. Higher temperatures support faster growth rates and enable some biota to attain significant populations (UNESCO/WHO/UNEP, 1996). Water temperature obtained during the sampling periods for all sites were insignificant at 95% confidence level and water temperature varies from 20.56 to 28.30°C. Higher values were recorded at SLW6 and sampling site; whereas, the

Table 2. Physical parameters result (Mean ± SD, n=6) at the sampling sites in Lake Hawassa.

Sampling site	pH	Temp (°C)	TDS (ppm)	DO (ppm)	Turbidity (NTUs)	EC (µS/cm)
SLW1	9.17 ± 0.05	25.3 ± 0.52	979.3 ± 1.5	7.84 ± 0.03	8.71 ± 0.1	1956 ± 1.7
SLW2	6.76 ± 0.4	21.33 ± 0.5	517.7 ± 0.6	4.76 ± 0.02	26.56 ± 1.2	1029.7 ± 1.2
SLW3	9.21 ± 0.04	20.6 ± 0.3	882.7 ± 1.1	5.43 ± 0.5	19.3 ± 0.9	1664.3 ± 6.0
SLW4	8.56 ± 0.1	24.5 ± 0.1	856 ± 2.6	8.59 ± 0.3	9.68 ± 0.2	1624 ± 4.5
SLW5	5.85 ± 0.1	25.5 ± 0.34	383.7 ± 0.6	8.07 ± 0.03	177.0 ± 1.2	741.7 ± 0.5
SLW6	8.16 ± 0.1	28.3 ± 0.1	912 ± 0.5	8.23 ± 0.1	8.37 ± 0.1	1831 ± 0.6
SLW7	8.86 ± 0.05	25.7 ± 0.05	833.3 ± 1.5	8.06 ± 0.1	27.7 ± 0.5	1842.3 ± 1.5
Average	8.67 ± 0.7	26.7 ± 2.0	928.3 ± 72.1	7.22 ± 0.9	47.9 ± 55.4	1851.4 ± 148
WHO (2004)	6.5 to 8.5	< 40.0	500	5.0 to 7.0	5.0	750
FAO (1985)	6.0 to 8.5	-	2000	> 4.0	-	3000

minimum value at SLW3 sampling site. There was a slight fluctuation in temperature that might be due to variation in the weather conditions. Nonetheless, temperature of Hawassa Lake water is likely suitable for aquatic lives.

Turbidity

Turbidity in natural waters is commonly caused by the presence of clay, silt, organic matter, algae, and other microorganisms (Lamb, 1985). The turbidity value of the sampling sites ranges from 8.37 to 177.0 NTUs with an overall mean value of 47.9 NTUs and this was higher than (WHO, 2004) standard for drinking purposes. The highest value of turbidity was recorded at SLW5 (177 ± 3.21 NTUs) followed by SLW7 sampling sites; whereas, the minimum value of turbidity was recorded at SLW6 (8.37 ± 0.14 NTUs) sampling site. The high values of turbidity could be mainly attributed to surface runoff from the catchment area as well as from inflowing perennial river loaded with silt during the sampling periods of small rainy season.

Electrical cconductivity (EC)

Electrical conductivity is a measure of how much total salt is present in the water. The more the ions existed, the higher the conductivity formed (Mosley et al., 2004). Electrical conductivity values range from 741.7 to 1956.0 µS/cm. The highest value was recorded at SLW1 sampling site, followed by SLW7, SLW6, SLW3, SLW4, and SLW2 sampling sites, respectively. These could be attributed to influx of dissolved solutes from the surrounding urban areas, agricultural fields and institutional effluents. All EC values recorded were higher than WHO standards for drinking purposes, except SLW5 (741.66 µS/cm) sampling site and lower than (FAO, 1985) standard for irrigation. The low value recorded at SLW5 might be due to adsorption of dissolved ions into organic particulates and suspended solids found in the river.

Total dissolved solids (TDS)

TDS emanating from the discharge of various chemicals used as food preservatives in food processing industry, ceramic and textile industry, waste from Hospitals, etc. The discharge of wastewater with a high TDS level into water bodies would have adverse impact on aquatic life and exacerbate corrosion in water networks (LVEMP, 2002). For all the other sampling sites, except for SLW5, the average value of TDS exceeds the maximum permissible limits (WHO, 2004) for the drinking purpose but within the limit given by FAO (1985) for irrigation water. The high value of TDS at these sampling sites were attributed to influx of dissolved solutes from agricultural fields, discharge of domestic waste from the town and other human activities like washing of clothes or different vehicle at and around the lake. Lower values of TDS below the WHO (2004) limits were observed at SLW5 sampling site and could be due to the dilution effect from the inflow of water during the sampling periods of small rainy season.

Dissolved oxygen (DO)

Oxygen is the main indicator of water quality in surface water. DO values in the present study ranged from 4.76 to 8.59 mg/L. The highest recorded values of DO were at SLW4 sampling site followed by SLW6 SLW5, SLW7, and SLW1 indicating the sampling sites were relatively free of organic waste during the study periods. However, lowest DO value was recorded at SLW2 (4.76 mg/L) and these values were below the permissible limits set by WHO and could be due to the decomposition of excess nutrient and biodegradable organic matter (Fikresilasie, 2011).

Table 3. Nutrient and BOD5, total hardness and alkalinity result (Mean ± SD, n=6) at the sampling sites in Lake Hawassa.

Sampling site	Nitrate (NO_3-)	Sulfate (SO_4^{2-})	Phosphate (PO_4^{3-})	Fluoride (F^-)	BOD5	Total Hardness	Total Alkalinity
	ppm	ppm	ppm	ppm	ppm	mg/L $CaCO_3$	mg/L $CaCO_3$
SLW1	4.3 ± 0.5	12.4 ± 0.7	1.26 ± 0.1	17.3 ± 0.7	63.4 ± 0.4	60 ± 2.0	14.6 ± 5.8
SLW2	3.13 ± 0.2	12.4 ± 0.4	1.31 ± 0.04	12.13 ± 0.7	168.2 ± 2.5	52.6 ± 1.1	14.6 ± 0.6
SLW3	3.43 ± 0.2	12.8 ± 0.4	0.3 ± 0.1	11.8 ± 0.9	159.0 ± 0.2	64 ± 0.5	11.3 ± 0.6
SLW4	4.71 ± 0.2	8.4 ± 0.1	1.33 ± 0.1	12.8 ± 0.4	161.2 ± 0.3	64 ± 1.0	11.3 ± 0.6
SLW5	2.83 ± 0.03	18.5 ± 0.6	1.9 ± 0.01	13.8 ± 0.4	153.1 ± 0.5	72.6 ± 1.1	19.3 ± 0.57
SLW6	3.68 ± 0.5	10.6 ± 0.3	1.34 ± 0.05	13.23 ± 0.8	156.5 ± 0.3	71.6 ± 1.5	14.3 ± 0.57
SLW7	6.79 ± 0.5	10.9 ± 0.5	1.36 ± 0.04	13.2 ± 0.6	74 ± 0.2	57.3 ± 1.5	10.0 ± 0.1
Average total	5.54 ± 1.8	11.6 ± 1.1	1.31 ± 0.1	15.3 ± 2.9	68.7 ± 7.5	58.6 ± 1.9	14.6 ± 3.3
WHO (2008)	45.0	250.0	0.1	1.5	2.0 - 5.0	300	120
FAO (1985)	50.0	400.0	2.0	-	8.0	-	-

Selected nutrients in sampled sites of Lake Hawassa

The mean concentrations of the selected nutrient, BOD5, total hardness and alkalinity are shown in Table 3. The mean values of the selected physical parameters ranged between 2.83 and 6.79 mg/L for nitrate, 8.4 and 18.5 mg/L for sulfate, 0.3 and 1.9 mg/L for phosphate, 11.8 and 17.3 mg/L for fluoride, 63.4 and 168.2 mg/L for BOD5, 52.6 and 72.6 mg/L $CaCO_3$ for total hardness, and 10.0 and 19.3 mg/L $CaCO_3$ for total alkalinity.

Nitrate-

The mean concentration of nitrate recorded at all sampling sites were within the limit of WHO (2008) and FAO (1985) standards. However, relatively highest concentration of nitrate was recorded at SLW7 (6.79 ± 0.5 mg/L) sampling site and this could be due to agricultural runoff and certain industrial wastes. The lowest nitrate concentration was recorded at SLW5 (2.83 ± 0.03 mg/L) sampling site showing that the sampling site was relatively less polluted by nitrogenous materials.

Sulfate

The mean concentration of sulfate recorded at all sampling sites were within the limit of WHO and FAO standards with the highest mean value measured at SLW5 (18.6 ± 0.6 mg/L) sampling site and the lowest at SLW4 (8.4 ± 0.1 mg/L) sampling site. High concentration of sulfate at SLW4 sampling site could be related to the discharge of sulfate containing municipal sewages and surface runoff that contain organic fertilizers from agricultural activities or due to the variability of the distribution of soluble sulfate salts in the sampling sites.

Orthophosphate

The mean concentration of orthophosphate recorded at all sampling sites were higher than the limit of WHO (2008) and lower than FAO (1985) standards with the highest mean value measured at SLW5 (1.90 ± 0.01 mg/L) sampling site. This could be due to pollution from domestic sewages, discharge of waste that led to eutrophication and surface runoff from phosphate containing fertilizers.

Fluoride

The mean concentration of fluoride recorded at all sampling sites was higher than the limit of WHO (2008) standards with the highest value measured at SLW1 (17.3 ± 0.7 mg/L) sampling site and the lowest at SLW3 (11.7 ± 0.3 mg/L) sampling site. Highest concentration of fluoride at the sampling sites prominently associated with a natural weathering of mineral bed rocks (WHO, 2008) or seepage of ground water into the lake. It is also a common problem mainly in rift valley lakes of Eastern Africa countries due to geological factors (Tamiru, 2006).

Table 4. Mean concentration (mean ± SD in mg/L, n=6) of metals at the sampling sites in Lake Hawassa.

Sampling site	Iron (Fe)	Magnesium (Mg)	Potassium (K)	Chromium (Cr)	Copper (Cu)	Zinc (Zn)	Manganes (Mn)
	ppm	ppm	ppm	ppm	ppm	ppm	ppm
SLW1	0.12 ± 0.03	29.0 ± 1.1	84.3 ± 0.1	0.17 ± 0.01	ND	7.4 ± 0.2	ND
SLW2	0.58 ± 0.03	26.8 ± 1.4	54.0 ± 1.1	0.3 ± 0.01	0.07 ± 0.01	1.1 ± 0.05	1.5 ± 0.05
SLW3	0.25 ± 0.02	19.8 ± 1.0	82.2 ± 0.7	0.45 ± 0.03	0.06 ± 0.01	1.5 ± 0.05	ND
SLW4	0.6 ± 0.1	32.2 ± 0.8	32.2 ± 0.8	0.42 ± 0.01	ND	3.0 ± 0.04	0.2 ± 0.01
SLW5	0.75 ± 0.1	24.2 ± 0.3	81.2 ± 1.5	0.3 ± 0.02	0.03 ± 0.02	0.4 ± 0.01	1.8 ± 0.01
SLW6	0.73 ± 0.04	26.3 ± 0.7	62.6 ± 0.3	0.58 ± 0.03	0.03 ± 0.02	0.2 ± 0.05	0.13 ± 0.01
SLW7	0.14 ± 0.03	26.3 ± 1.1	64 ± 0.3	0.26 ± 0.02	0.03 ± 0.02	4.1 ± 0.1	0.16 ± 0.01
Average total	0.13 ± 0.01	27.6 ± 1.9	74.2 ± 14.3	0.22 ± 0.06	0.05 ± 0.03	5.75 ± 2.3	0.83 ± 0.9
WHO (2008)	0.3	30.0	20.0	0.05	2.0	5.0	0.1
FAO (1985)	-	120.0	-	-	-	-	-

Total hardness

The total hardness of water recorded at all sampling sites was lower than the limit of WHO (2008) standards with the highest mean value measured at SLW5 (72.6 ± 1.1 mg/L $CaCO_3$) sampling site and could be due to industrial effluents, and urban and rural runoff. The lowest total hardness value recorded at SLW2 (52.6 ± 1.1 mg/L $CaCO_3$) sampling site.

Total alkalinity

The alkalinity of surface water is primarily a function of carbonate, hydroxide content and includes the contributions from borates, phosphates, silicates and other bases. Total alkalinity measures the ability of water to neutralize the acids. The total alkalinity of water recorded at all sampling sites was lower than the limit of WHO (2008) standards with the highest mean value measured at SLW5 (19.3 ± 0.57 mg/L $CaCO_3$) and the lowest value at SLW7 (10.0±0.1 mg/L $CaCO_3$). Highest value of total alkalinity at the sampling sites prominently associated with waste discharge and microbial decomposition of organic matter in the sampling sites.

Biochemical oxygen demand (BOD_5)

The mean concentration of value of BOD_5 was the highest at SLW2 (Tikurwuha River) (168.2 ± 2.5 mg/L) followed by SLW4 (Fikir Hayik) (161.2 ± 0.3 mg/L), SLW3 (Near Haile Resort) (159.0 ± 0.2 mg/L), and SLW6 (Near Lewi Resort) (156.5 ± 0.3 mg/L). The lowest BOD_5 value recorded at SLW1 (Near Airport) and SLW7 (Around Loke) were 63.4 ± 0.4 and 74 ± 0.2 mg/L, respectively. The values of BOD5 recorded at all sampling sites exceed the maximum permissible limits of WHO and FAO standards. These could be due to continued discharge of domestic waste from the city, industries, agricultural activities, and waste from fish market that is near to the lake and other human activities that could produce organic wastes.

Metals in sampled sites of Lake Hawassa

The mean concentrations of the selected metals concentration are shown in Table 4.

Metals concentration

The mean concentration of major and trace metals analyzed ranged between 0.12 and 0.75 mg/L for Iron, 19.8 and 32.2 mg/L for Magnesium, 32.2 and 84.3 mg/L for Potassium, 0.17 and 0.58 mg/L for Chromium, 0.03 and 0.07 mg/L for Copper, 0.2 and 7.4 mg/L for Zinc, and 0.13 and 1.8 mg/L for Manganese. Lead and cadmium were not detected in all sampling sites as their concentration was below the detection limit (0.04 mg/L for Pb and 0.01 mg/L for Cd) of Buck Scientific, Model 210 VGP Atomic absorption spectrophotometer.

Magnesium

The average values of major metals concentration were in the following descending order: K > Mg > Fe. The recorded value for magnesium concentrations lies within the prescribed limit of WHO and FAO except at SLW4 (32.2 ± 0.8 mg/L) sampling site and could be originated from industrial effluents containing salts of magnesium or other magnesium sources carried by runoff from rural agricultural lands and urban wastewater. The minimum concentration of magnesium was recorded at SLW3 (19.8 ± 1.0 mg/L) sampling site.

Potassium

The average concentration of potassium exceeds the maximum permissible limits of WHO (2008) in all of the sampling sites. Highest potassium concentration recorded at SLW1 (84.3 ± 0.1 mg/L) sampling site followed by SLW3, SLW5, SLW7, SLW6, SLW2, and SLW4 sampling sites. This could be due to the effect of hospital effluents, septic system, and other anthropogenic activities besides the natural sources (Worako, 2015) or waste fruits and vegetables containing high-level potassium could be another source.

Iron

The concentrations of iron recorded at all sampling sites exceed the maximum permissible limits of WHO standard. Highest iron concentration recorded at SLW5 (0.75 ± 0.1 mg/L) sampling site followed by SLW6, SLW4, SLW2, SLW3, SLW7, and SLW1 sampling sites. This could be due to corrosion of metallic materials made of iron and from a certain industrial processes.

Copper

In two sampling sites (SLW1 and SLW4), copper was not recorded. The maximum concentration of copper were recorded at SLW2 (Tikurwuha River) (0.07 ± 0.01 mg/L) and SLW3 (Near Haile Resort) (0.06 ± 0.01 mg/L) sampling sites that exceeded WHO standard and could be due to incineration of waste, industrial discharge, sewage disposal and antifouling paints (Moore et al., 2013). However, the concentrations of copper in the rest of the sampling sites were within the maximum permissible limits of WHO standard.

Zinc

The concentrations of zinc recorded at all sampling sites except at SLW1 (7.4 ± 0.2 mg/L), were within the maximum permissible limits of WHO (2008) standard and could be due to storm water draining from vehicle oil, grease and lubricants spill on roads, vehicle repairing and washing areas as well as from industrial effluent containing leached zinc from pipe coatings, or raw chemicals used up by industries (EEPA, 2003).

Manganese

Highest concentration of manganese was recorded at SLW5 (1.80 ± 0.01 mg/L) and SLW2 (1.5 ± 0.05 mg/L) sampling sites which exceeded WHO standard. Manganese was not detected in SLW1 and SLW3 sampling sites and the lowest concentration of manganese was recorded at SLW6.

Chromium

The concentrations of chromium recorded at all sampling sites exceed the maximum permissible limits of WHO standard. Highest chromium concentration recorded at SLW6 (Near Lewi Resort) (0.58 ± 0.03 mg/L) sampling site followed by SLW3 (Near Haile Resort), SLW4, SLW2, SLW5, SLW7, and SLW1 sampling sites. These might be attributed to industrial discharge from pigments, paints, ceramic, glass and leather tanning industries as well as domestic wastewater composed of grey water that may consist of: the bath, dishwasher products, personal care products and laundry detergents; which are good sources of these metal elements (Tjandraatmadja et al., 2008).

Comparison of results with previous work

In the present study, seven sampling sites were selected to determine the physico-chemical water quality parameters of the lake but in the previous studies ten sampling sites (Abate et al., 2015) and four sampling sites (Praveen and Mukemil, 2015) were selected. The physico-chemical and biological water quality characteristic of the lake Hawassa analyzed by different researchers in different periods of time is shown in Table 5.

The concentration of iron, manganese, copper, lead, and chromium in the previous studies were within the permissible limit set by WHO (2008) standard or else not detected at all. However, in the present study the concentration of these metals exceeded WHO limit for drinking purpose. These might be due to the accumulation of these metals into the lake through effluent discharge from ceramic, textile and leather tanning industries located along the streams that fed into Tikurwuha River (Berehanu et al., 2015).

Both in the present and previous study, the

Table 5. Mean values of physico-chemical water quality parameters of Hawassa Lake reported by researchers.

Parameter	Worako AW (2015)	Abate et al. (2015)	Praveen and Mukemil (2015)	Present work (2019)
pH	7.54	7.54	7.67	8.67
Temperature	21.2	21.2	25.7	26.7
DO	17.8	17.8	16.9	7.22
BOD5	117	117	-	68.7
TDS	450.1	450.1	547.5	928.3
EC	750	750	806.3	1851.4
Turbidity	8.44	8.44	11.5	47.9
Total hardness	121.9	121.9	-	58.6
Total alkalinity	-	-	--	14.6
Nitrate	5.27	5.27	14.7	5.54
Sulfate	-	-	-	11.6
Phosphate	1.12	1.12	-	1.31
Fluoride	12.8	12.8	12.1	15.3
Potassium	74.1	74.1	-	74.2
Magnesium	28.1	28.1	26.2	27.6
Iron	0.085	0.085	0.06	0.13
Manganese	0.09	0.09	0.004	0.83
Zinc	0.19	0.19	-	5.75
Copper	0.01	0.01	-	0.05
Lead	ND	ND	-	ND
Chromium	ND	ND	-	0.22
Cadmium	ND	ND	-	ND

All units except temperature (°C), turbidity (NTUs), SC (µS/cm), and pH (in pH scale) are in mg/L. Total hardness and alkalinities are expressed as mg/L of $CaCO_3$. ND: Not detected.

concentration of potassium, phosphate, and fluoride were found to be higher than the limit of WHO (2008) standards. These could be due to effluent discharge from Hawassa Referral Hospital (Abate et al., 2015), Resorts and hotels, domestic sewages or surface runoff from phosphate containing fertilizers. Turbidity of the lake exceeded WHO standard and it has shown an increase in its value through time. These might be due to a steady increase in suspended sediment due to a polluted tributary and surface runoff or the development of an algal bloom on the lake. A decrease in the concentration of DO was observed as time goes by. And these might be due to the decomposition of accumulated organic waste by microbial that deplete the concentration of oxygen. In all of these studies, the value of pH, temperature, total hardness, nitrate, sulphate and magnesium were found to be within the permissible limit set by WHO.

Conclusion

The study has shown that the concentration of metals such as manganese, zinc, chromium and nutrients like phosphate, BOD5 were found above the recommended WHO (2008) standard for drinking purpose and this could have an adverse impact on aquatic life and humans and animals that uses the lake water for various purpose. Elevated levels of these metals and nutrients could be due to point source pollution from ceramics, textile, plastics, leather tanning and food processing industries located near the rivers and streams that end up into the lake. Thus, Hawassa City Administration should take measures to check the effluents of those industries in order to meet the requirements of effluent discharge limits and prohibitions. Furthermore, the lake also faces non-point source pollution caused by urban stormwater, agricultural runoff, over grazing, deforestation, soil erosion and land development as it was indicated by elevated levels of TDS, EC, turbidity, fluoride and potassium. As a result, Hawassa City Administration along with other NGOs, physical soil and water conservation measures with ultimate intention of reducing sever soil erosion and its associated impact in communal and private lands of the upper catchments of Lake Hawassa watershed should be put in place in order to rehabilitate the condition of the lake. Nonetheless, the condition of the lake will continue to deteriorate unless intervention measures are put in place.

CONFLICT OF INTERESTS

The authors have not declared any conflict of interests

ACKNOWLEDGEMENTS

The authors thank the Rift Valley Lakes Basin Branch Authority of Hawassa, Ethiopia, for their cooperation. They also thank Hawassa University for supporting the research.

REFERENCES

Abate B, Woldesenbet A, Fitamo D (2015). Water quality assessment of Lake Hawassa for multiple designated water uses. Water Utility Journal 9:47-60.

Ayenew T (2007). Water management problems in the Ethiopian rift: Challenges for development. Journal of African Earth Sciences 48(2):222-236.

Ayenew T, Becht R, Lieshout A, Gebreegziabher Y, Legesse D, Onyando J (2007). Hydrodynamics of topographically closed lakes in the Ethio-Kenyan Rift: the case of lakes Awassa and Naivasha. Journal of Spatial Hydrology 7(1).

Berehanu B, Lemma B, Tekle-Giorgis Y (2015). Chemical Composition of Industrial Effluents and Their Effect on the Survival of Fish and Eutrophication of Lake Hawassa, Southern Ethiopia. Journal of Environmental Protection 6:792-803.

Delzer GC, McKenzie SW (2003). Five-day biochemical oxygen demand: U.S. Geological Survey Techniques of Water-Resources Investigations, book 9, chap. A7 (3d ed.), section 7.0, accessed February, 2019, from http://pubs.water.usgs.gov/twri9A/.

EEPA (2003). Guideline Ambient Environment Standards for Ethiopia. Prepared by EPA and UNIDO under ESDI project US/ETH/99/068/Ethiopia, Addiss Ababa.

Food and Agriculture Organization (FAO) (1985). Water Quality for Agriculture. Food and Agriculture Organization. Rome, Italy.

Fikresilasie T (2011). Impact of brewery effluent on river water quality: the case of Meta Abo Brewery Factory and Finchewa River in Sebeta, Ethiopia. Addis Ababa University Laibraries. URI: http://localhost:80/xmlui/handle/123456789/7407.

Gebremedhin K, Berhanu T (2015). Determination of some selected heavy metals in fish and water samples from Lake Hawassa and Ziway Lakes. Science Journal of Analytical Chemistry 3:10-16.

Girma T, Ahlgren G (2009). Seasonal Variations in Phytoplankton biomass and primary production in the Ethiopian Rift Valley lakes, Ziway, Awassa and Chamo-The basis of fish production. Elsevier Science, Limnologica 40:330-342.

HALCROWind (2008). Rift Valley Lakes Basin Integrated Resources Development. Master Plan Study Project, Draft Phase 2 Report Part II Prefeasibility Studies, Halcrow Group Limited and Generation Integrated Rural Development (GIRD) consultants. Unpublished report. Addis Ababa. http://open_jicareport.jica.go.jp/pdf/12066403_03.pdf

Katie G (2011). Environmental Policy Review: Lake Water Management in three Ethiopian Rift Valley Watersheds.

Lamb JC (1985). Water Quality and its control. John Wiley and sons.

Larissa D, Mesfin M, Elias D (2012). Assessment of heavy metals in water samples and tissues of edible fish species from Awassa and Koka Rift Val Lakes, Ethiopia. Environmental monitoring Assessment 185(4).

Legesse D, Vallet-Coulomb C, Gasse F (2003). Hydrological response of a catchment to climate and land use changes in Tropical Africa: case study South Central Ethiopia. Journal of Hydrology 275:67-85.

LVEMP (2002). Integrated water quality/limnology study of Lake Victoria. Final technical report, COWI/DHI, Denmark. https://www.oceandocs.org/bitstream/handle/1834/7149/ktf0090.pdf?sequence=1&isAllowed=y

Makin MJ, Kingham TJ, Waddams AE, Birchall CJ, Teffera T (1975). Development Projects in the Southern Rift Valley of Ethiopia. Land resource study no., 21. England: Land Resource Division, Ministry of Overseas Development.

Moore RB, Milstead WB, Hollister JW**,** Walker HA (2013). Estimating Summer Nutrient Concentrations in Northeastern Lakes from SPARROW Load Predictions and Modeled Lake Depth and Volume. PLoS ONE 8(11):e81457.

Mosley L, Sarabjeet S, Aalbersberg B (2004). Water quality monitoring in Pacific Island countries: Handbook for water quality managers & laboratories, 1st Edition. ISSN: 1605-4377: SOPAC, The University of the South Pacific. Suva Fiji Islands.

Mulugeta DB (2013). The Impact of Sedimentation and Climate Variability on the Hydrological Statur of Lake Hawassa, South Ethiopia. Dissertation, Bonn, Rheinische Friedrich-Wilhelms-Universität Bonn. Photometer instructional manual for Palintest test, https://www.palintest.com/en/products/photometer-7100

Praveen M, Mukemil KO (2015). CME water quality index and assessment of physico-chemical parameters of Lake Hawassa, Ethiopia. International Journal of Recent Scientific Research 6(6):7891-7894.

Tamiru A (2006). Ground water occurrence in Ethiopia, Addis Ababa. UNESCO P 75.

Tjandraatmadja G, Diaper C, Gozukara Y, Burch L, Sheedy C, Price G (2008). Sources of priority contaminants in domestic wastewater: Contaminant contribution from household products. Commonwealth Scientific and Industrial Research Organisation (CSIRO): Water for a Healthy Country National Research Flagship.

United Nations Educational, Scientific and Cultural Organization (UNESCO) World Healthorganization (WHO) United Nations Environment Programme (UNEP) (1996). Water Quality Assessments - A Guide to Use of Biota, Sediments and Water in Environmental Monitoring, 2nd Edition. P 651.

Walakira P, Okot-Okumu J (2011). Impact of Industrial Effluents on Water Quality of Streams in Nakawa-Ntinda, Uganda. Journal of Applied Sciences and Environmental Management 15(2):289-296.

World Health Organization (2008). Guidelines to drinking water quality. 3rd ed., 1:1-666. Geneva. https://www.who.int/water_sanitation_health/dwq/fulltext.pdf

World Health Organization (2004). Guidelines for drinking-water quality. 3rd ed., 1: Geneva. https://www.who.int/water_sanitation_health/dwq/GDWQ2004web.pdf

Worako AW (2015). Physicochemical and biological water quality assessment of Lake Hawassa for multiple designated water use. Journal of Urban and Environmental Engineering 9(2):146-157.

Zinabu GM, Zerihun D (2002). The chemical composition of the effluent from Awassa Textile Factory and its effects on aquatic Biota. Ethiopian Journal of Science 25(2):263-274.

Vol. 11(7), pp. 129-142, July-September 2019
DOI: 10.5897/IJWREE2019.0837
Article Number: 628E5C461761
ISSN: 2141-6613

http://www.academicjournals.org/IJWREE

ACADEMIC JOURNALS
expand your knowledge

International Journal of Water Resources and Environmental Engineering

Full Length Research Paper

Enhancing the adsorption of Pb(II) and Fe(II) in the reactor by the thermally treated alluvial clay from Far North Cameroon

Adjia Zangué H.[1,2*], Nga B.[2], Kamga R.[2], Villiéras F.[1] and Ebio Nko'o G.[3]

[1]Laboratoire Interdisciplinaire des Environnements Continentaux (LIEC) UMR 7360 CNRS-Université de Lorraine 15 Avenue du Charmois, 54500 Vandœuvre-lès-Nancy, France
[2]National School of Agro-Industrial Sciences (ENSAI) University of Ngaoundere B.P. 455 Adamaoua, Cameroon.
[3]Department of Chemistry, Faculty of Science (FS) University of Ngaoundere B.P. 454 Ngaoundere, Cameroon.

Received 28 January, 2019; Accepted 25 April, 2019

The objective of this work was to investigate the influence of the thermal treatment of alluvial clay on the ad-sorption capacity of Pb(II) and Fe(II) to reduce clogging during adsorption phenomenon. The chemical, X- ray diffraction (XRD), Fourier transform infrared spectroscopy (FTIR), scanning electron microscope (SEM) and transmission electron microscopy (TEM) analysis of the alluvial clays reveal that the main mineral present is smectite, kaolinite and quartz. Cation exchange capacity (CEC) and specific surface area of the raw clay fraction are 62 meq/100 g and 104 m2/g respectively. The mains oxydes of alluvial clay fraction<50µm are SiO2, Al2O3 and Fe2O3.The adsorbent used in this work is the alluvial clay, that after splitting has been thermally treated at 300°C and 600°C, the natural clay properties does not completely disappear until 300°C and 600°C. This study shows that the losses are about 3% for the heat treatment at 300°C (A300) and 5% for the heat treatment at 600°C (A600) after fractionation of Alluvial clays. The adsorption equilibrium is reached in five minutes, whatever the pH, temperature and the molar ratio of the solution. The pH is increased the removal increases as seen from plots of 2, 4 and 6 which gave removals as high as 92.15µmol/g and 100.6 µmol/g to Pb(II) and 92.68 µmol/g and 110.5 µmol/g to Fe(II) respectively. The temperature is decreased the removal increases as seen from plots of 50°C, 40°C and 30°C which gave removals as high as 99.8 µmol/g and 100.3 µmol/g to Pb(II) and 98.9 µmol/g and 100.3 µmol/g to Fe(II) respectively. While, the adsorption capacity was increased as decreasing the temperature. So, it is be recognized that adsorption mechanism should be physical adsorption. The adsorption process of Pb(II) and Fe(II) are best described by the second-order equation. However, the adsorption isotherms could be well fitted by the Freundlich equation, proves the surface heterogeneity of thermally treated Alluvial Clay.

Key words: Adsorption, agitated reactor, thermally treated alluvial clay, Cameroon.

INTRODUCTION

The pollution of water and/or soil, accidentally and/or voluntarily, by some chemicals of industrial origin (phenols, hydrocarbons, dyes ...) or agricultural (pesticides, fertilizers ...) constitutes a source of environmental degradation and is currently of particular interest internationally (Bouras, 2003; Demin et al., 2013).

Recent industrial revolution in central Africa as

Cameroon has enormously increased the industrial wastewater production which is highly contaminated with various types of heavy metals. Heavy metal contamination exists in waste effluents of different factories such as metal plating, mining operations, tanneries, ceramic painting, manufacturing paints, catalysts, alloy industries, galvanizing iron, polymer stabilizer, storage batteries manufacturing, pesticides, wood preservation, pigments factories and families cloths painting (Basso et al., 2002; Sundar et al., 2010; Arwidsson et al., 2010; Berthelot et al., 2008; Cao et al., 2008; Moon et al., 2010; Chrastný et al., 2010). Heavy metals have been acknowledged as potential health and environmentally hazardous materials. Many studies have shown that these metals are toxic even at low concentrations. The presence of these toxic metals can in turn, cause accumulative poisoning, destroy liver, cancer and brain damage when found above the tolerance level (Arif et al., 2015; Geier et al., 2015; Carneiro et al., 2014; Chen et al., 2012; Ilyin et al., 2010; Bridges and Zalups, 2010; Ilyin et al., 2002, 2003; CACAR, 2003; Carretero et al., 2002; Chang, 1977). Additionally, another problem in our study area is the presence of iron on the soil and this iron migrated in water process. Presently, many techniques such as chemical precipitation, extraction, reverse osmosis and adsorption are being used for the removal of heavy metals from wastewater. Adsorption technique is an economical process especially using low cost adsorbents. Many investigators have evaluated natural clay and the date pits as low-cost adsorbents due to their adsorption properties for heavy metals including cobalt, lead, cadmium, zinc and chromium ions (Ahmad et al., 2011, 2018; Sameeh et al., 2016; Abdullah et al., 2017; Ahmad et al., 2018). In contrast, there are very few studies on the mineralogy and use of clays from vertisol of the northern region of Cameroun. None of the above studies are dealing with alluvial clay of the far north region of Cameroon. In fact, Adjia et al. (2014) discovered new adsorbent, alluvial clay as alternative solution to resolve waste water problem.

Lead and iron are considered dangerous micropollutants. In fact, Lead is the heavy metal and Iron is presented on the littoral soil, affects processing water, and decreases by this fact the rentability of the industries in this economical area of Cameroon.

The toxicity affected by these heavy metals is considered high even in trace amounts (IARC, 1992; Curren et al., 2015). Given the variable quality of the contaminated water and the harmful effects of pollution, this metal as micropollutant is reduced by adsorption on the alluvial clay. Using alluvial clays as adsorbents is of interest in the removal of pollutants. This is justified by the importance of the surface developed by this material, by the presence of negative charges on the surface, by the possibility of exchange of the cations and by a wide availability in nature (Adjia et al., 2014).

However, many studies showed that, during the adsorption phenomenon in the reactor we have the clogging problem (Vishal et al., 2013). The aim of this work is to investigate the influence of heat treatment of a Alluvial clay on its adsorption capacity of Pb (II) and Fe (II) in the reactor.

MATERIALS AND METHODS

Alluvial clay materials

Study area and sampling

The soil samples were taken in a dry river bed situated between the towns of Maroua and Kaele in the far-north region of Cameroun (Picture 1). The system coordinates of this area is 10°02.883N and 014°23.084E. The climate is tropical-dry, characterized by 7- 8 months of dry season and 4 - 5 months of wet season. The mean annual rainfall and temperature in the area is 800 mm and 28.5°C, respectively. During the wet season, the rivers (locally call Mayo) contain running water while in the dry season there is almost no water. The soil depth during the sampling is 99 cm (**Adjia et al., 2013, 2014**).These soil samples were packaged in plastic packaging.

The soil fraction <50 µm (A50)

In this study, we focused on the size fraction <50 µm. The soil aggregate is pulverized in a mortar and then homogenized. About 1 kg of this sample is soaked in 2 L of distilled water for 4 h. This mixture is homogenized by subjecting to wet sieving with a 50-µm mesh sieve. The water is then removed by drying at 105°C in an oven for 24 h. The solid obtained was treated with 5% hydrogen peroxide solution to eliminate organic matter. The dried fraction is sprayed in an Agathe mortar; the powder obtained is weighed and stored in a sealed jar; and the clay fraction <2 µm (A02) was extracted by sedimentation. However, especially in this work, the resulting mixture was then sieved over 50-µm (A50) mesh sieve.

Mineralogy and physicochemical properties

X-ray diffraction (XRD): The X-ray diffraction (XRD) data were obtained using a D8 Bruker diffractometer with $CoK\alpha_1$ radiation (λ= 1.789 Å). Spectra were recorded on oriented and unoriented samples. The detection limit for a given crystalline phase is estimated at around 1% in mass. Ethylene glycol and heat treatments (550°C) were used to provide additional information essential for the identification of clay minerals.

Fourier Transform Infra Red (FTIR): Infrared spectra were recorded using an IFS 55 Bruker Fourier transform IR spectrometer equipped with an MCT detector (6000 to 600 cm^{-1}) cooled at 77K and in diffused reflectance (Harrick attachment) mode. The amount. of clay was 70 mg dispersed in 370 mg KBr

*Corresponding author E-mail: hzangue42@gmail.com.

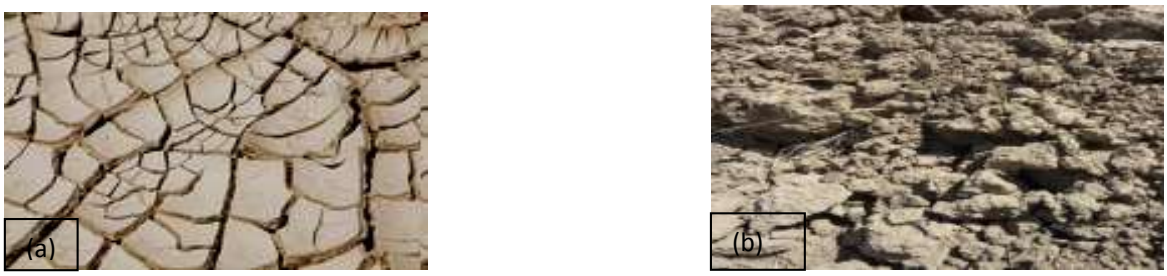

View A

View B (10°02883N et 014°23.084E)

Picture 1. View A: a) Mayo dried up; b) place of sampling. View B: a) sampling method.

Scanning and transmission electron microscopy: TEM observations were conducted with a Philips CM20 microscope equipped with an EDS detector. Secondary and backscattering SEM observations were carried out on a Hitachi 2500 LB SE microscope equipped with a Kevex Delta EDS spectrometer. SEM was used to assist in the identification of individual accessory minerals incorporated in the clay samples by comparing their morphological characteristics with their elemental compositions.

Chemical analyses: These were performed on the two clay fractions. The major elements were determined by inductively coupled plasma atomic emission spectroscopy (ICP-AES), whereas trace elements and rare earths elements were determined by inductively coupled plasma mass spectrometry (ICP-MS).

Cation exchange capacities (CEC): These were measured using cobaltihexamine [$Co(NH_3)_6Cl_3$] as exchangeable ions. The amount of cobaltihexamine fixed by the solid phase was determined from concentration measurements using UV-vis spectroscopy. The displaced cations were determined by atomic absorption spectrometry (Perkin-Elmer 1100B). The equilibrium pHs of clay suspensions were determined using a standard LPH 330 T electrode.

Textural properties: Nitrogen adsorption-desorption isotherms at 77K were recorded on a step-by-step automatic home-built set up. Pressures were measured using 0-1000 Pa and 0-100.000 Pa Baratron-type pressure sensors provided by Edwards. The nitrogen saturation pressure was recorded in situ using an independent 0-100.000 Pa Baratron-type pressure sensor provided by Edwards. Prior to adsorption, the samples were outgassed overnight at 120°C and under residual pressure of 0.01 Pa. Nitrogen N55 (purity > 99.9995%) used for experiments was provided by alphagaz (France). Specific surface areas (SSA) were determined from adsorption data by applying the Brunauer-Emmet-Teller (BET) equation and using 16.3Å^2 for the cross sectional area of nitrogen. In the present study, error in the determination of the SSA was estimated as +/- 1 m^2/g. Micropores volumes and non-microporous surface areas were obtained using the t-plot method proposed by De Boer et al. (1996). Pore size distributions were calculated on the desorption branch using the Barrett-Joyner-Halenda method, assuming slit-shaped pores.

Heat treatment

The treatment is carried out using a muffle furnace. It consists in weighing the crucible empty, then putting 159.94 g of alluvial clay fraction in the crucible, weighed, and then the sample was introduced into the oven at different temperatures from room temperature (25±1°C) to the temperature set for 40 min at 300°C and 70 min at 600°C. Finally, it was allowed to cool and the samples weighed again.

Experimental procedures

Lead salts ($Pb(NO_3)_2$) and Mohr salt ($Fe(NH_4)_2(SO_4)_2,6H_2O$) are used for the preparation solutions, using waste water conditions. All experiments were carried out at pH 7.0 (except when the effect of pH was studied). The pH of each solution was adjusted to the desired value by addition of dilute HCl or NaOH solutions.

Preparation of solutions and Adsorption phenomenon

The initial lead solution at 4826µmol/L was prepared by dissolving 0.81g of lead nitrate salt ($PbNO_3)_2$ hydrated in 500ml of distilled water. The resulting solution was stored in a one-liter flask. This solution has been diluted to provide solutions of desired concentrations during adsorption.

The initial solution of 17851 µmol/L Iron was prepared by dissolving 3.5 g of hydrated Mohr salt ($Fe(SO_4)_2(NH_4)_2(SO_4)_2,6H_2O$) in 500 ml of distilled water. The resulting solution was stored in a one-liter flask.

For the adsorption experiments, 25 ml of lead nitrate solution (289.6 µmol/L) and Mohr salt at a concentration of 1071.4 µmol/L are introduced into a 50-ml series of Erlenmeyer flasks. The whole solution is kept at ambient temperature (25 ±1°C) and stirred with a water bath at a constant speed of 120 rpm. Subsequently, 0.25 g of alluvial clay of each sample is introduced into each Erlenmeyer flask. These are then stirred at approximately 60 rpm at constant temperature for a period of one hour. At each time interval, the contents of the Erlenmeyer flask are filtered on Whatman N°1 filter paper. The optical density read at the visible spectrophotometer is converted into concentration and the amount of lead and iron adsorbed per unit mass of alluvial clay is given by the relation

$$q_{e=(C_o-C_e)}\frac{V}{m_{adsorbant}}\ (mg/g) \quad (1)$$

Where, qe is the amount of the metal adsorbed; C_0 is the initial concentration of the solution (µmol/L); C the concentration of the solution at time t in (µmol/L); m is the mass of alluvial clay used in (g) and V is the volume of the solution in (mL). The wavelength of 539 nm was used for Pb(II) analysis and 510 nm for Fe(II) analysis.

Effect of pH: The work is carried out in a pH range of between 2 to 6 in steps of 2 to observe the difference of the amounts adsorbed in an acidic.

Effect of temperature: To measure the influence of temperature, we will have three temperatures between 30 and 50°C, initial concentration, adsorbent and normal pH. Temperature has two major effects on the adsorption process.

Modeling of adsorption kinetics: Adsorption kinetics were studied using the pseudo-first-order, pseudo-second-order and intraparticular diffusion equations.

i) Kinetic model of pseudo-first order: The velocity equation of the pseudo-first-order kinetic model is given by the relation:

$$\log(q_e - q_t) = logq_e - \frac{k_1 t}{2{,}303} \quad (2)$$

Where q_e and q_t are respectively the relative amounts adsorbed at the adsorption equilibrium at time t, and k_1 (min^{-1}) is the pseudo-first order rate constant. Representing the log (q_e – q_t) = f(t) function, we obtain a straight line of slope - $\frac{k}{2.303}$ and an intercept of log qe (Harouna et al., 2015).

ii) Kinetic model of pseudo-second order: The pseudo-second-order kinetic model can be represented in the following form:

$$\frac{t}{q_t} = \frac{1}{k_2 q_e^2} + \frac{t}{q_e} \quad (3)$$

Where q_e and q_t are respectively the relative quantities adsorbed at equilibrium and at time t, k_2 is the pseudo-second-order rate constant (Harouna et al., 2015).

iii) Kinetic model of intra particle diffusion: The intraparticular diffusion model can be represented by the equation:

$$q_t = k_{int}\sqrt{t} + C \quad (4)$$

Where q_t is the relative amount of adsorbed Lead and Iron at time t, k_{int} is the intraparticular diffusion constant and C is a constant **(Reddy et al., 2010)**. The regression of the function $q_t = f(\sqrt{t})$, makes it possible to obtain a line of slope k_{int} and ordinate at the origin C.

Modeling adsorption isotherms: The adsorption capacity was determined using the isotherms of Langmuir and Freundlich.

i) Langmuir model: The theory proposed by Langmuir is based on a homogeneous distribution of the adsorption sites. The Langmuir isotherm can be represented by the equation:

$$q_e = \frac{aK_L C_e}{1+K_L C_e} \quad (5)$$

Where C_e is the residual relative amount at the adsorption equilibrium, q_e, the relative amount of the adsorbed Lead and Iron per gram of adsorbent has the adsorbed amount for the monolayer and K_L the equilibrium adsorption constant (Domga et al., 2015).

ii) Freundlich model: The simple and empirical model of Freundlich is the second most commonly used model. It is considered that it applies to many cases, especially in the case of an adsorbent with a heterogeneous adsorption surface (energetically different adsorption sites).

$$q_e = K_F C_e^{\frac{1}{n}} \quad (6)$$

The linear expression of the Freundlich equation is obtained by taking the logarithm of the equation:

$$lnq_e = lnK_F + \frac{1}{n} lnC_e \quad (7)$$

Where K_F and *n* are the constants respectively reflecting the measurement of the adsorption capacity and the adsorbent-adsorbate affinity (Harouna et al., 2015).

RESULTS AND DISSCUSION

Mineralogy and physicochemical properties

X-ray diffraction

XRD patterns of alluvial clay samples show that it consists predominantly in smectite, kaolinite and quartz, with accessory minerals such as anatase, microcline, albite and rutile (Figure 1a). Results of the ethylene glycol test on oriented clay fraction showed the characteristic displacement of the basal peak of smectite from 15.2 to 18.3 Å (Figure 1b). The usual displacement of the smectite from 15.2 to 10.1Å on heating at 550°C is also observed. All the vertisol profiles in this area showed a similar mineralogical composition; however, Adjia et al. (2013, 2014) found that most of the smectite minerals of the vertisol soil of this zone are mixtures of montmorillonite and beidellite. The spectra of the A50

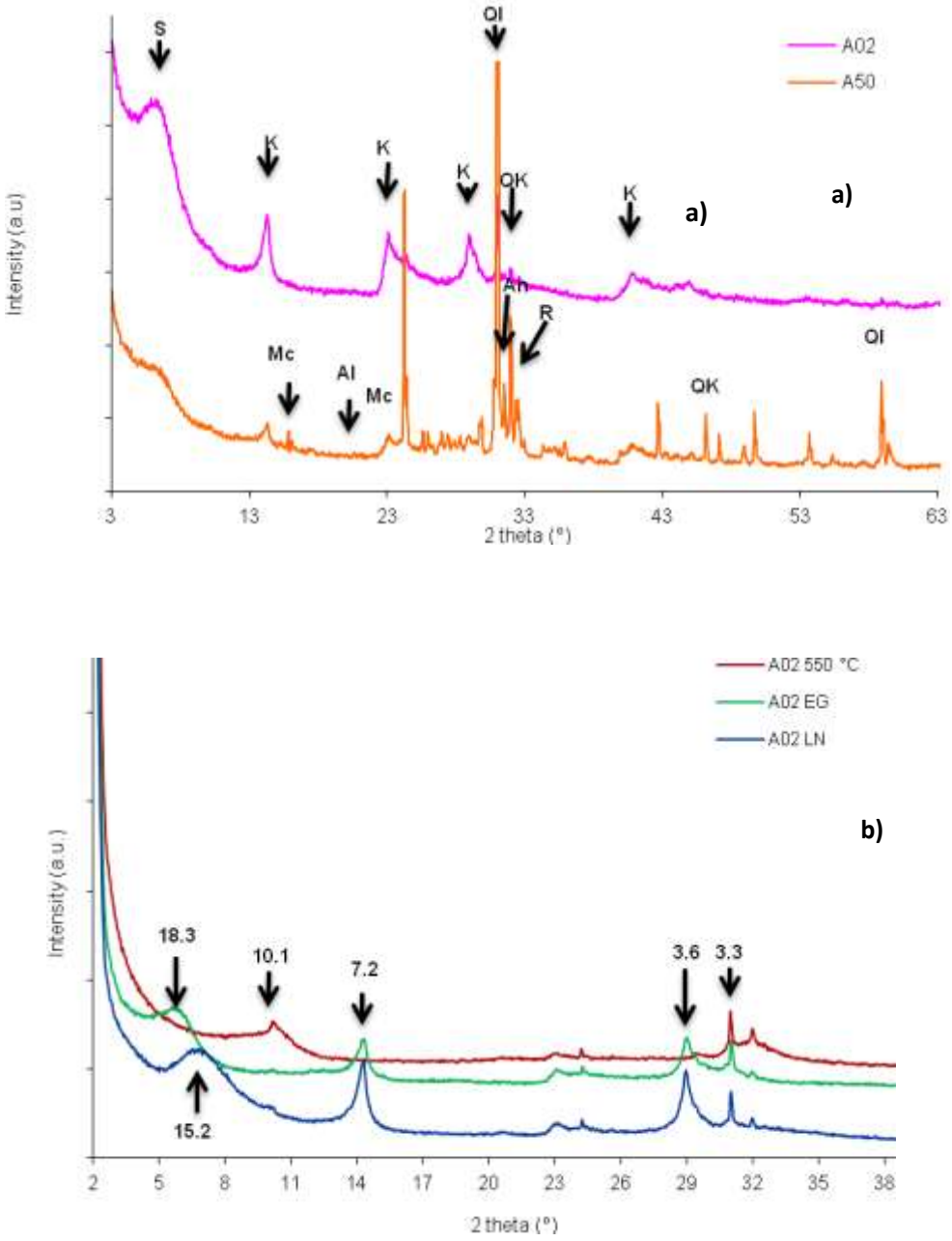

Figure 1. a) X-ray diffraction patterns of a) natural (A02, A50), **b)** oriented preparation of clay fraction (A02 LN), (A02 EG), (A02 550°C). Basal spacings on fig.1b are given in Å. Legend: (S: smectite ; K : kaolinite ; Mc : microcline ; Al : albite ; Q : quartz ; An : anatase ; R : rutile; I: illite)

fraction show a well-defined peak of quartz indicating a high amount of quartz in this sample. On the contrary, the clay fraction only presents very few amount of quartz.

Infrared spectroscopy

The infrared spectra of the two clays fractions are presented in Figure 2. The two spectra have almost the same feature. IR analysis confirms that smectite and kaolinite are the main mineral present in our clay samples. The broad band at 3390 cm^{-1} is usually attributed to the adsorbed water at the interlayer of smectite clays. The band at 1612 cm^{-1} is also attributed to smectite interlayer water. The band at 3698 cm^{-1} is assigned to the OH stretching vibration of kaolinite, whereas the band at 3620 cm^{-1} is characteristic of the OH stretching of kaolinite and of AlAlOH or AlMgOH groups

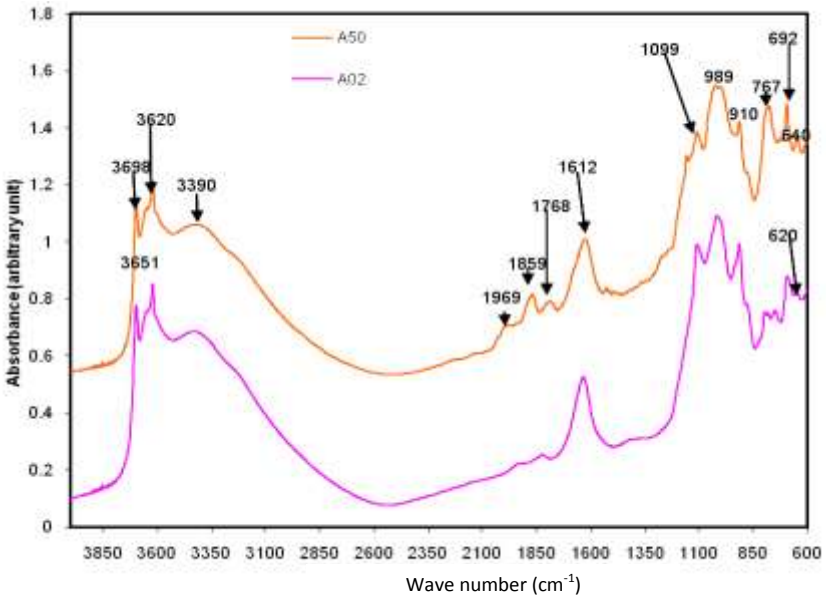

Figure 2. Infrared spectrum of the Alluvial Clay A02 and A50.

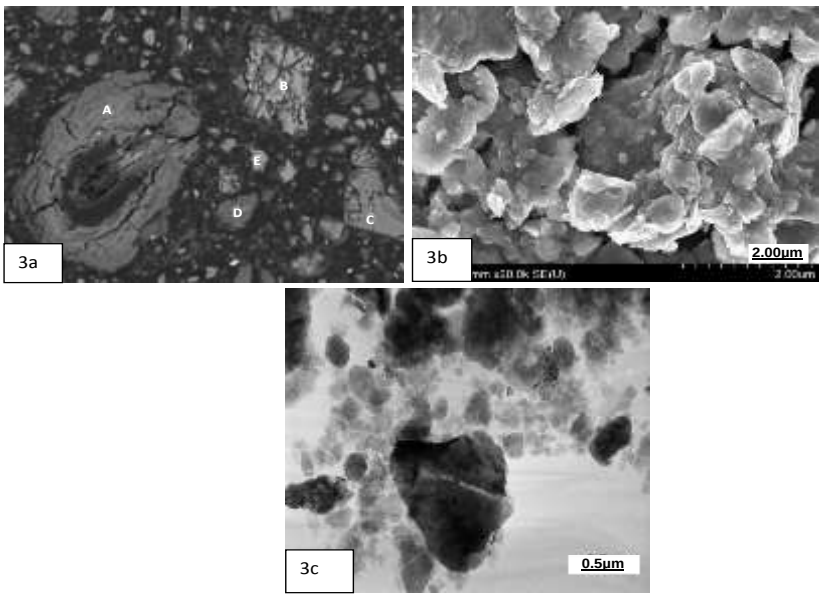

Figure 3. Scanning electron photomicrograph (SEM) and TEM micrograph of alluvial clayey fraction , showing typical texture.**3a)** SEM A50 (polished slide of clay embedted in resins); **3b)** SEM A50 (powder) ; **3c)** TEM A02. Minerals identification is derived from EDX analyses.

of smectite. In addition, IR analysis shows the absence of calcium or magnesium carbonates and of organic matter in the studied samples.

Scanning and transmission electron microscopy

SEM observation on a polish slide of A50 fraction shows large aggregates and small particles dispersed over the entire matrix (Figure 3a). SEM with EDX analysis of the aggregates reveal the presence of smectite [A]: (Si/Al≈0.60), of microcline [B]: (Si/Al≈2.8 and 3), of quartz [C]: (Al=0), of interstratified [D]: (Si/Al≈1.6) and of kaolinite [E]: (Si/Al≈2). Those minerals have currently been identified from XRD and IR analyses. The SEM images of A50 powder shows the usual cluster of rose

Table 1. Chemical analysis of major elements on a sandy fraction <50 µm (A50) and clayey fraction< 2 µm (A02).

Sample (%)	SiO_2	Al_2O_3	Fe_2O_3	MnO	MgO	CaO	Na_2O	K_2O	TiO_2	P_2O_5	LOI	Total
A02	46.37	22.88	9.21	0.04	1.27	0.87	0.56	1.05	1.26	0.08	16.5	100.0
A50	60.66	17.04	5.88	0.09	0.75	0.77	0.94	3.18	1.34	0.06	9.45	100.1

Note: LOI: loss on ignition.

Table 2. Equilibrium pH, cation exchange capacities (CEC), and exchangeable cations of the clay fraction on a sandy fraction <50 µm (A50) and clayey fraction< 2 µm (A02).

Samples	pH±0.1	CEC (chem) meq/100 g ± 5	CEC (UV) meq/100 g ±5	Na^+ (meq/100 g)± 2	K^+ (meq/100 g)± 1	Ca^{2+} (meq/100 g)± 2	Mg^{2+} (meq/100 g) ± 1
A02	9.2	58	62	14.8	1.5	29.2	13.0
A50	9.5	31	34	6.3	0.6	15.8	6.3

Note: Chem: derived from chemical analysis of displaced cations. UV: derived from the measurement of cobaltihexamine concentrations by UV-visible spectroscopy.

shaped aggregates of smectite particles (Figure 3b). TEM-EDX analysis confirms the presence of kaolinite and smectite; and also reveals the additional presence of quartz, feldspar and iron oxy-hydroxides as minor phases (Figure 3c) (Adjia et al., 2013).

Chemical analyses

The major element composition of the alluvial clay fraction is presented in the Table 1 below. The main oxides of alluvial clay fraction <50 µm are SiO_2, Al_2O_3 and Fe_2O_3. The high amount of SiO_2 in the alluvial clay fraction<50 µm is related to its high content in quartz as compared to the alluvial clay fraction. Small amount of MnO, MgO, CaO, Na_2O, K_2O, TiO_2 and P_2O_5 are also found in the two samples. This implied that Mg^{2+}, Ca^{2+} and Na^+ are exchangeable cations of the alluvial clays samples (Adjia et al., 2013).

Physico-chemical characteristics of the alluvial clay

The cation exchange capacity (CEC) values measured from variation in concentration of cobatihexamine match those deduced from the chemical analysis of exchangeable cation for all the samples described herein. This confirms the absence of soluble phases in the studied fraction. The CEC of the clay fraction (Table 2) lie between the values reported in the literature for smectite, that is, 60 to 150 meq/100 g (Adjia et al., 2014). The lower CEC value for A50 fraction compared to clay fraction correlates with its lower content in clays. Indeed, the CEC ratio between A50 and A02 is 0.54, in good agreement with the 57% of clays in A50. From the analyses of the cations exchanged with cobaltihexamine, it can be concluded that around 2/3 of the layer charge is compensated by divalent cations (Ca^{2+} and Mg^{2+}) (Adjia et al., 2013).

Textural

The adsorption-desorption isotherms on the two samples reported in Figure 4 are typical of clay materials containing smectites (Neaman et al., 2003). Numerical values deduced from the adsorption and desorption isotherm are given in Table 3. The difference in the specific surface areas (SSA) of A02 and A50 fractions can be attributed to their quartz content. In fact, A50 fraction contains a large amount of quartz, and quartz particles present low specific surface areas compared to clays. Indeed, the 0.54 SSA ratio between A50 and A02 samples is also consistent with CEC and clay content of A50 showing that sandy fraction of A50 has no surface area. Microporosity represent about 20% of the total surface area and can be assigned to clay layers organisation as generally observed in the case of swelling clays with divalent exchangeable cations (Adjia et al., 2014).

Influence of pH

It appears from Figure 5 that the kinetics of adsorption kinetics of Pb(II) are all the same pace. The balance is reached in less than 5 min, implying that equilibrium had been reached. The amount of Pb(II) adsorbed increases with pH. The amount adsorbed at equilibrium is of the same order for the two samples. The type of thermally

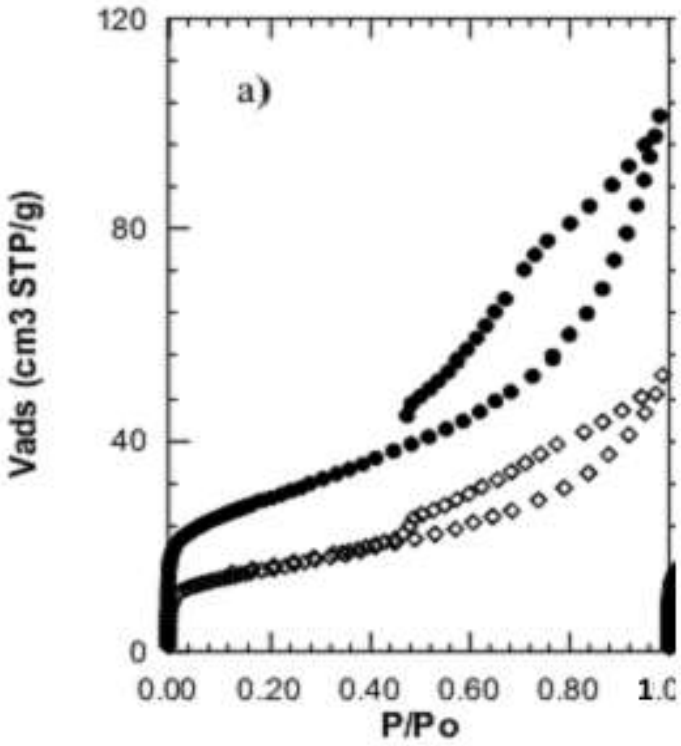

Figure 4. Nitrogen adsorption and desorption isotherms at 77K. For a)clay fraction (A02) and sandy fraction (A50) **●: A02 ; ◊: A50.**

Table 3. Textural parameters deduced from N_2 adsorption desorption isotherms (SSA: specific surface area) on a sandy fraction <50 µm (A50) and clayey fraction< 2 µm (A02).

Samples	BET C constant	BET SSA (m^2/g) ±1	Non Microporous surface area (m^2/g) ± 1	Microporous equivalent surface area (m^2/g) ± 1	Microporous Volume (cm^3/g) ± 0.0003
A02	215	103	82	26	0.0091
A50	337	56	44	15	0.0053

Note: SSA: specific surface a

treatment of alluvial clay and salts solutions do not influence this adsorption. However, as the pH is increased, the removal increases as seen from plots of 2, 4 and 6 which gave removals as high as 92.15 and 100.6 µmol/g to Pb(II) as well as 92.68 and 110.5 µmol/g to Fe(II) respectively (Figures 5 and 6). As shown, the maximum biosorption capacity was reached at pH 6 with 100.6 µmol/g to Pb(II) and 110.5 µmol/g to Fe(II), respectively for lead and iron concentration.

As for Pb(II) and Fe(II) in Figure 6, adsorption equilibrium is rapidly reached (92.15 and 92.68 µmol/g). However, the influence of the pH is less marked, with the adsorption done in the same way with the pH 2, 4 and 4. At pH values higher than 7, Fe(II) precipitation occurred. One notes an increase of the quantities adsorbed by 11% when one passes from the pH 4 until the pH 6.

The alluvial clays are known to possess a negative surface charge in solution. As pH changes, surface charge also changes, and the sorption of charged species is affected (attraction between the positively charged metal ion and the negatively charged clay surface). The effect of pH can be explained in terms of pHzpc (zero point of charge) of the adsorbent. Below this pHzpc, the surface charge of the adsorbent is positive. An increase in pH above pHzpc shows a slight increase in adsorption in which the surface of the adsorbent is negatively charged and the sorbate species are still positively charged. The increasing electrostatic attraction

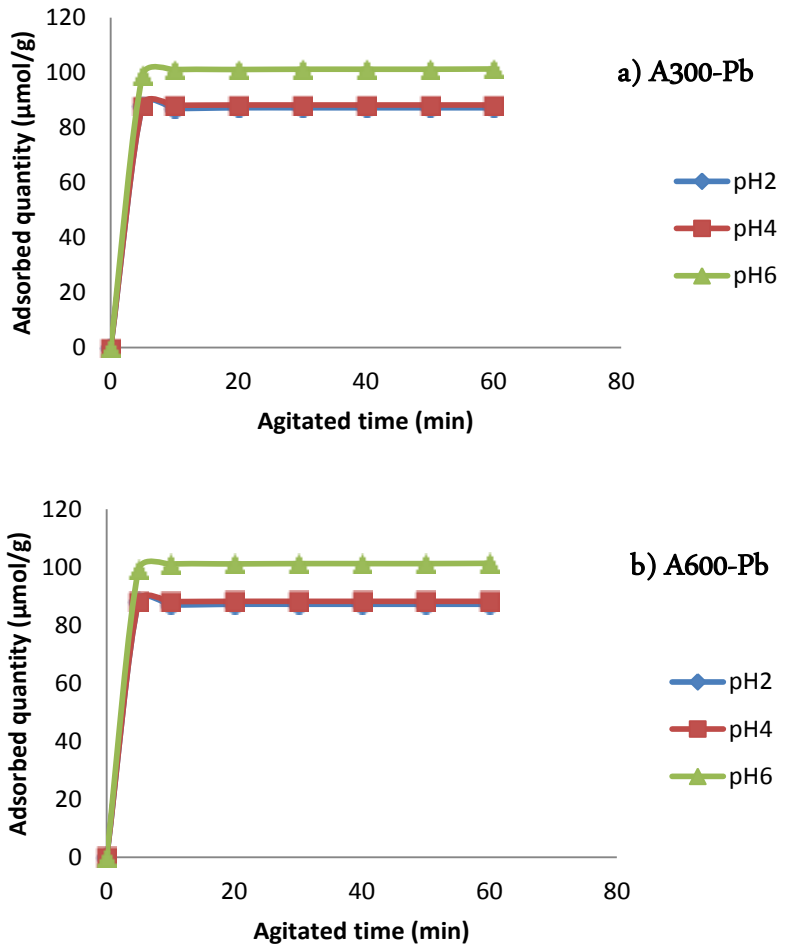

Figure 5. Effect of pH on the kinetics of adsorption of Pb(II) by the treated Alluvial clay thermally at a) 300°C (A300) and b) 600°C (A600): pH=2; pH=4 and pH=6.

between positive sorbate species and adsorbent particles would lead to increased adsorption of metal ions (Kadirvelu et al., 2001).

Influence of temperature

As the temperature is decreased the removal increases as seen from plots of 50, 40 and 30°C which gave removals as high as 99.8 and 100.3 µmol/g to Pb(II) as well as 98.9 and 100.3 µmol/g to Fe(II) respectively. It can be concluded from Figures 7 and 8 that decreasing the temperature increases adsorption. The maximum adsorptions of Pb(II) and Fe(II) ions on thermally treated alluvial clay were found at T= 30°C “to A300 and A600 of Pb(II)” and T= 30°C “to A300 and A600 of Fe(II)”, respectively. Consequently, it is clear that adsorption equilibrium is not a thermo-dependent process, because the alluvial clay is thermally treated. This is mainly because of increased surface activity suggesting that adsorption between metal ion and alluvial clay is an exothermic process (Yasemin and Zübeyde, 2006; Johnson, 1990). Meanwhile, the adsorption capacity was increased as the temperature decreases. So, it should be recognized that the adsorption mechanism is physical.

Modeling the kinetics of adsorption

This helps to investigate the possible mechanisms involved in the adsorption of theoretical Pb(II) and Fe(II) intraparticle diffusion, pseudo-first order and pseudo-second order.

Intraparticular and pseudo-first order diffusion models are not applicable for the explanation of the adsorption of Pb(II) and Fe(II) by our thermally treated alluvial clays at 300 and 600°C given the low values of the R^2 coefficients for these models (Table 4). The coefficients of determination R^2 for the pseudo-second-order kinetic model are close to 1 regardless of the alluvial clay

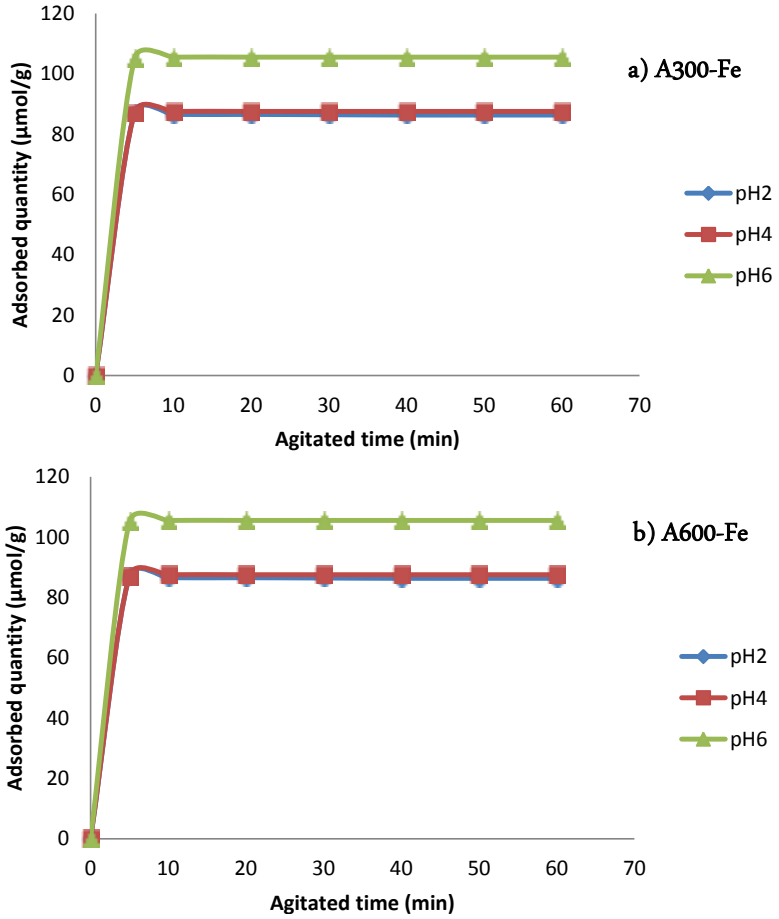

Figure 6. Effect of pH on Fe(II) adsorption kinetics by thermally treated Alluvial clay at a) 300°C (A300) and b) 600°C (A600): pH=2; pH=4 and pH=6.

sample. This shows that the pseudo-second-order kinetic model is particularly suitable for describing the adsorption kinetics of Lead and Iron by our thermally treated alluvial clays at 300 and 600°C.

The first-order kinetic process has been used for reversible reaction with an equilibrium being established between liquid and solid phases (Low et al., 2000). Whereas, the second -order kinetic model assumes that the rate-limiting step may be chemical adsorption (Wu et al., 2001), in many cases, the second-order equation correlates well to the adsorption studies (Sağ and Aktay, 2002). It is more likely to predict that the adsorption behaviour may involve valency forces through sharing of electrons between transition metal cations and adsorbent.

Modeling isothermal adsorption

The Langmuir and Freundlich models are often used to describe equilibrium sorption isotherms. The most widely used Langmuir equation, which is valid for monolayer sorption on to a surface with a finite number of identical sites, is given by Equation 5. The widely used empirical Freundlich equation based on sorption on a heterogeneous surface is given by Equation 6. The calculated results of the Langmuir and Freundlich isotherm constants are given in Table 5. It is found that the adsorptions of Pb(II) and Fe(II) on thermally treated alluvial clay correlated well (R > 0.99) with the Langmuir equation as compared to the Freundlich equation under the concentration range studied. The essential features of a Langmuir isotherm can be expressed in terms of a dimensionless constant separation factor or equilibrium parameter, R_L which is used to predict if an adsorption system is ‘‘favourable’’ or ‘‘unfavourable’’. The separation factor, R_L is defined by:

$$RL = \frac{1}{1+bC0} \quad (8)$$

where C_0 is the initial Pb(II) or Fe(III) concentration (ppm) and b is the Langmuir adsorption equilibrium constant ($ml.mg^{-1}$). Table 6 lists the calculated results. Based on the effect of separation factor on isotherm shape, the R_L

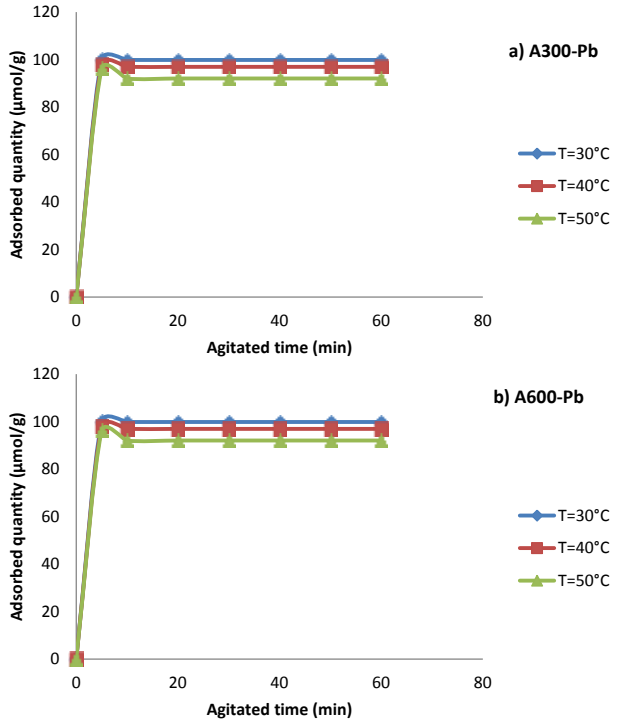

Figure 7. Effect of temperature on the adsorption kinetics of Pb(II) by thermally treated Alluvial clay at a) 300 ° C (A300) and b) 600 ° C (A600): T = 30°C, T = 40°C and T = 50°C.

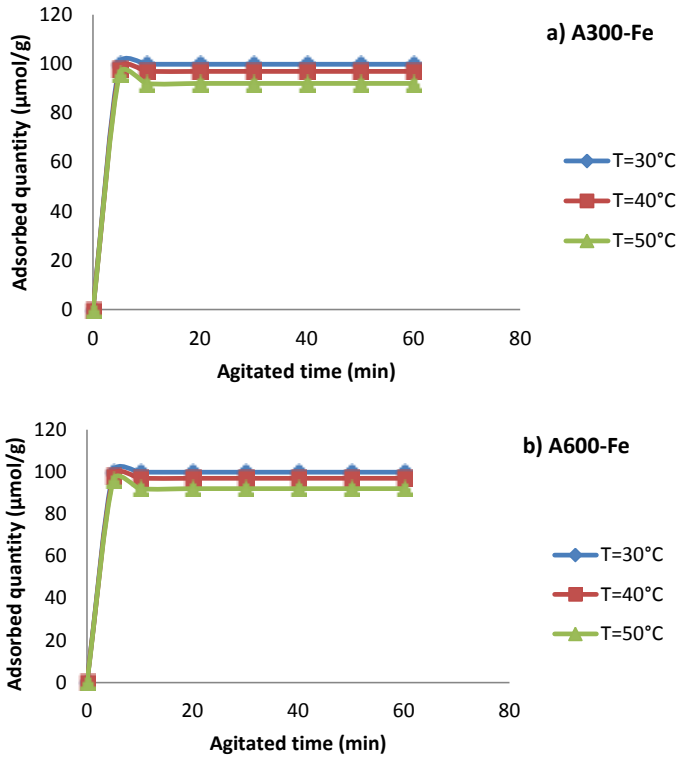

Figure 8. Effect of temperature on Fe(II) adsorption kinetics by thermally treated Alluvial clay at a) 300°C (A300) and b) 600°C (A600): T = 30°C, T = 40°C and T = 50°C.

Table 4. Parameters of kinetic models for the adsorption of lead and iron on thermally treated Alluvial Clay 300°C (A300) and 600°C.

Adsorbents	pH	Lead Pseudo-second order			Iron Pseudo-second order		
		q_{ecal}(µmol/g)	k_2	R^2	q_{ecal}(µmol/g)	k_2	R^2
A300	2	19.92	0.21	0.998	91.74	0.1980	0.999
	4	23.42	0.2145	0.999	93.46	0.1431	0.999
	6	27.55	0.2635	0.999	104.16	0.9216	0.999
A600	2	18.73	0.3752	0.999	91.74	0.0792	0.999
	4	22.32	1.1150	0.999	91.74	0.0848	0.999
	6	26.25	2.0737	0.999	103.09	0.0724	0.999

Table 5. Values of Langmuir and Freundlich isotherms constants.

Pollutants	Adsorbents	Langmuir isotherm			Freundlich isotherm		
		q_m(µmol/g)	b	R^2	n	K_F	R^2
Lead	A300	16.584	-0.063	0.998	1.427	1.062	0.962
	A600	18.620	-0.300	0.982	1.504	1.026	0.981
Iron	A300	94.339	-0.898	0.998	1.054	1.022	0.992
	A600	90.090	-0.572	0.997	1.111	1.016	0.994

values are in the range of $0 < R_L < 1$, which indicates that the adsorptions of Pb(II) and Fe(II) on thermally treated alluvial clay are favourable. Thus, thermally treated alluvial clays are favourable adsorbers. Indeed, the Langmuir model indicates that we have a homogeneous distribution of adsorption sites while the model shows that our adsorbent has a surface heterogeneity.

Conclusion

In this study, enhancing the adsorption of Pb(II) and Fe(II) by the thermally treated alluvial clay from far north Cameroon in the reactor was examined, including equilibrium and kinetic studies. In a view to evaluate their potential use as adsorbent for wastewater treatment, the mineralogical and physico-chemical properties of alluvial clays from far north region of Cameroon has been determined. The alluvial clays reveal that the main mineral present is smectite, kaolinite and quartz. Cation exchange capacity (CEC) and specific surface area of the raw clay fraction are 62 meq/100 g and 104 m^2/g respectively. The main oxides of alluvial clay fraction<50 µm are SiO_2, Al_2O_3 and Fe_2O_3. The overall formula of the clay mineral which was established are: smectite, $[Si_{3.42}Al_{0.58}]_{tetra}[Al_{0.87}Fe_{0.96}Mg_{0.17}]_{octa}\ O_{10}(OH)_2(C^+)_{0.75}$; and kaolinite, $Si_2Al_{1.95}Fe_{0.05}O_5(OH)_4$.

As the pH is increased, the removal increases as seen from plots of 2, 4 and 6 which gave removals as high as 92.15 and 100.6 µmol/g to Pb(II) and 92.68 and 110.5 µmol/g to Fe(II) respectively. As the temperature is decreased the removal increases as seen from plots of 50, 40 and 30°C which gave removals as high as 99.8 and 100.3 µmol/g to Pb(II) and 98.9 and 100.3 µmol/g to Fe(II) respectively. Meanwhile, the adsorption capacity was increased as the temperature decreases. So, it should be recognized that adsorption mechanism is physical. The adsorption process of Pb(II) and Fe(II) are best described by the second-order equation. In our case, the second-order equation correlates well to the adsorption studies. It is more likely to predict that the adsorption behaviour may involve valency forces through sharing of electrons between transition metal cations and adsorbent. However, the adsorption isotherms could be well fitted by the Freundlich equation, which proves the surface heterogeneity of thermally treated alluvial clay. The R_L values are in the range of $0 < R_L < 1$, which indicates that the adsorptions of Pb(II) and Fe(II) on thermally treated alluvial clay are favourable. The clogging is not the problem during adsorption phenomenon in agitated reactor with thermally treated alluvial clay. Finally, the thermally treated alluvial clay, as low cost adsorbent is a favourable adsorber for a growing country.

CONFLICT OF INTERESTS

The authors have not declared any conflict of interests.

ACKNOWLEDGEMENTS

The authors are grateful to all members and teachers of the Applied Chemistry Laboratory ENSAI, Department of Chemistry (FS) for the efforts made towards the success of this work.

REFERENCES

Abdullah A, Moonis AK, Hameed BH, Ayoub AA, Masoom RS, Zeid AA, Yacine B, HadjA (2017). Mercerized mesoporous date pit activated carbon—A novel adsorbent to sequester potentially toxic divalent heavy metals from water. PloS one 12(9):e0184493

Adjia H, Zangué FV, Kamga R (2014). Dépollution des eaux usées par les argiles alluviales. Editions à EUE d'un livre, Référence du livre : 978-613-1-59387-1 (ISBN 978-613-1-59387-1); ISBN-10: 6131593876; EAN: 9786131593871; Maison d'édition: Editions universitaires europeennes; Site Web: http://www.editions-ue.com/; Publié le:18-09-2014.

Adjia H, Zangué FV, Kamga R, Thomas F (2013). Mineralogy and physico-chemical properties of alluvial clays from far-north region of Cameroon: A tool for an environmental problem. International Journal of Water Resources and Environmental Engineering 5(1):54-66, January 2013 Available online at http://www.academicjournals.org/IJWREE DOI: 10.5897/IJWREE12.117 ISSN 1991-637X ©2013 Academic Journals.

Ahmad T, Rafatullah M, Ghazali A, Sulaiman O, Hashim R, Ahmad A (2011). Oil palm biomass based adsorbents for the removal of water pollutants—a review. Journal of Environmental Science and Health, Part C 29:177-222.

Ahmad T, Mohammad D, Mohammad R, Arniza G , Othman S, Rokiah H, Mohamad N, Mohamad I (2018). The use of date palm as a potential adsorbent for wastewater treatment: a review, Environmental Science and Pollution Research 19:1464-1484 DOI 10.1007/s11356-011-0709-8.

Arif TJ , Mudsser A , Kehkashan S , Arif A , Inho C, Qazi M. Rizwanul H (2015). Heavy Metals and Human Health: Mechanistic Insight into Toxicity and Counter Defense System of Antioxidants. International Journal of Molecular Sciences (ijms) 29592-29630. International Journal of Molecular Sciences 16:29592-29630.

Arwidsson Z, Elgh-Dalgren K, von Kronhelm T, Sjöberg R, Allard B, van Hees P (2010) Remediation of heavy metal contaminated soil washing residues with amino polycarboxylic acids. Journal of Hazardous Materials 173:697-704.

Johnson BB (1990). Effect of pH, Temperature and concentration on the adsorption cadmuin on gethite. Environmental Science and Technology 24(1):112-118.

Berthelot Y, Valton E, Auroy A, Trottier B, Robidoux PY (2008). Integration of toxicological and chemical tools to assess the bioavailability of metals and energetic compounds in contaminated soils. Chemosphere 74:166-177.

Bouras O (2003). Thèse de doctorat, Ecole Doctorale Sciences Technologie et Santé, Faculté des Sciences et Techniques, Université de Limoge (2003).

Bridges CC, Zalups RK (2010). Transport of inorganic mercury and methylmercury in target tissues and organs. Journal of Toxicology and Environmental Health, Part B 13(5):385-410.

CACAR (2003): Canadian Contaminants Assessment Report II, Sources, Occurrence, Trends and Pathways in the physical environment, Northern Contaminants program, Minister of Indian Affairs and Northern Development, Minister of Public Works and Government Services Canada P 332.

Cao X, Dermatas D, Xu X, Shen G (2008). Immobilization of lead in shooting range soils by means of cement, quicklime, and phosphate amendments. Environmental Science and Pollution Research 15(2):120-127.

Carneiro MFH; Oliveira SJM; Grotto D, Batista BL, de Oliveira Souza, VC; Barbosa F Jr. (2014). A systemic study of the deposition and metabolism of mercury species in mce after exposure to low levels of Thimerosal (ethylmercury). Environmental Research 134:218-227.

Chang LW (1977) Neurotoxic effects of mercury: A review. Environmental Research 14:329-373.

Chen CW, Chen CF, Dong CD (2012). Distribution and Accumulation of Mercury in Sediments of Kaohsiung River Mouth, Taiwan. APCBEE Procedia 1:153-158.

Chrastný V, Komárek M, Hájek T (2010). Lead contamination of an agricultural soil in the vicinity of a shooting range. Environmental Monitoring and Assessment 162:37-46.

Coetzee PP, Coetzee LL, Puka R, Mubenga S (2003). Charac-terisation of selected South African clays for defluoridation of natural waters. Water SA 29:331-338.

Curren MS, Liang CL, Davis K, Kandola K, Brewster J, Potyrala M, Chan HM (2015). Assessing determinants of maternal blood concentrations for persistent organic pollutants and metals in the eastern and western Canadian Arctic. Science of the Total Environment 527/528:150-158.

Da Costa ACA., Antunes WM, Luna AS, Henriques CA (2003). An evaluation of copper biosorption by a brown seaweed under optimized conditions. Electronic Journal of Biotechnology 6(3):174-184.

De Boer JH, Linsen BG, et Osinga TJ (1996). Studies on pore systems in catalysts. VI. The universal curve. Journal of Catalysis 4:643-648.

Domga R, Harouna M, Tcheka C, Tchatchueng JB, Tsafam A, Domga, Kobbe DN, Dangwang D (2015). Batch Equilibrium, Kinetic and Thermodynamic Studies on Adsorption of Methylene Blue in Aqueous Solution onto Activated Carbon Prepared from *Bos Indicus Gudali* Bones, Chemistry Journal 1(6):172-181.

Geier DA, King PG, Hooker BS, Dorea JG, Kern JK, Sykes LK, Geier, MR (2015).Thimerosal: Clinical,epidemiologic and biochemical studies. Clinica Chimica Acta 444:212-220.

Harouna M, Tcheka C, Abia D, Kobbe DN, Loura BB, Tchatchueng JB (2015). Kinetic, Thermodynamic and Equilibrium Studies on Adsorption of Alumina and Zinc Ions onto Activated Carbon from Hull Seeds of Moringa Oleifera, International Journal of Engineering Research and Science and Technology 4(4):164-172.

International Agency for Research on Cancer (IARC) (1992). Heavy metals in the environmental health: toxicity and carcinogenicity, IARC Scientfic Publications n°118, Lyon 1992.

Ilyin I, Ryaboshapko A, Afinigenova O, Berg T, Hjellbrekke AG, Lee DS (2002). Lead, cadmium and mercury transboundary pollution in 2000. MSC-E/CCC Technical Report 5/2002.

Ilyin I, Rozovskaya O, Travnikov O, Aas W, Hettelingh JP, Reinds GJ (2003). Heavy metals: transboundary pollution of the environment. EMEP Status report, 2(2003):40.

Sundar K, Vidaya R, Amitava M Chandrasekaran N (2010). High Chromium tolerant bacterial strains from palar river basin : Impact of tannery pollution. Research Journal of Environmental and Earth Sciences 2(2):112-117, 2010 ISSN:2041-0492.

Kadirvelu K, Thamaraiselvi K, Namasivayam C (2001). Adsorp-tion of nickel(II) from aqueous solution onto activated carbon prepared from coirpith. Separation and Purification Technology 24:497-505.

Low KS, Lee CK, Liew SC (2000). Sorption of cadmium and lead from aqueous solutions by spent grain. Process Biochemistry 36:59-64.

Basso MC, Cerrella EG, Cukierman AL (2002). Lignocellulosic Materials as Potential Biosorbents of Trace Toxic Metals from Wastewater. Programa de Investigación y Desarrollo de Fuentes Alternativas de Materias Primas y Energía (PINMATE), Departamento de Industrias, Facultad de Ciencias Exactas y Naturales, Universidad de Buenos Aires, Intendente Guiraldes 2620, Ciudad Universitaria, 1428 Buenos Aires, Argentina Industrial & Engineering Chemistry Research 41(15):3580-3585 DOI: 10.1021/ie020023h Publication Date (Web): June 26, 2002 Copyright © 2002 American Chemical Society.

Moon DH, Cheong KH, Kim TS, Khim J, Choi SB, Ok YS, Moon OR (2010). Stabilization of Pb contaminated army firing range soil using calcinated waste oyster shells. Journal of Korean Society of Environmental Engineers 32(2):185-192.

Neaman A, Pelletier M, Villieras F (2003). The effects of exchanged cation, compression, heating and hydration on textural properties of bulk bentonite and its corresponding purified montmorillonite. Applied

Clay Science 22(4):153-168.
Reddy HKD, Ramana DKV, Seshaiah K, Reddy AVR (2010). Biosorption of Ni(II) from aqueous phase by Moringa oleifera bark, a low cost biosorbent. Desalination, pp 8.
Sağ Y, Aktay Y (2002). Kinetic studies on sorption of Cr(VI) and Cu(II) ions by chitin, chitosan and Rhizopus arrhizus. Biochem. Engineering Journal 12:143-153.
Sameeh AM, Reham IM, Amina RA (2016). Removal of heavy metals from aqueous solutions by means of agricultural wastes: assessments based on biological assay and chemical analysis. Journal of Bio Innovation 5(4):480-505, 2016|ISSN 2277-8330 (Electronic).
Vishal KC, Balakrishman P, Deshmukh SK, Vishal IK (2013). Evaluation of adsorption mechanism in clogging of materials used in drip irrigation system. Journal of Agricultural Engineering 50(3):51-56.
Wu FC, Tseng RL, Juang RS (2001). Enhanced abilities of highly swollen chitosan beads for color removal and tyrosinase immobilization. Journal of hazardous materials 81(1-2):167-177.
Yasemin B, Zübeyde B (2006). Removal of Pb(II) from wastewater using wheat bran. www.elsevier.com/locate/jenvman. Journal of Environmental Management 78:107-113.

Related Journals: